RSC Advances

REVIEW

View Article Online
View Journal | View Issue

Cite this: *RSC Adv.*, 2026, **16**, 12768

Recent advances in enhancing the luminescence efficiency of rare earth upconversion nanoparticles for biomedical applications

Chenxi Guo,†[a] Yishan Ding,†*[b] Xinyu Cheng,[a] Ting Zhou,[a] Zhihua Xu,[a] Alang Zhang[a] and Feng Shi *[a]

Rare earth upconversion nanoparticles (UCNPs) have made remarkable progress in overcoming the limitations of traditional optical probes in biomedical applications, such as shallow tissue penetration and strong background interference, owing to the anti-Stokes luminescence properties of near-infrared excitation followed by visible/ultraviolet emission. In this review, we systematically summarized the core luminescence mechanisms, including excited-state absorption, energy transfer upconversion, photon avalanche, and other multipath energy transfer processes, and discussed the optimization progress of the co-precipitation, sol–gel method, hydrothermal, and thermal decomposition methods. This review focused on the latest achievements in improving luminous efficiency through strategies such as core–shell structure design, ion doping regulation, and surface functionalization. In biomedicine, UCNPs have been used for the high-resolution imaging of deep tissues, high-sensitivity biosensing, and precise photodynamic therapy. Moreover, this article systematically reviewed the latest research progress on the biomedical applications of UCNPs. Finally, we proposed a development direction in material design innovation and clinical translation to provide a reference for promoting the development of UCNPs from laboratory research to practical applications.

Received 22nd September 2025
Accepted 16th December 2025

DOI: 10.1039/d5ra06977g

rsc.li/rsc-advances

1. Introduction

The study of the optical properties of multivariate nanomaterial systems has always been of importance. With the in-depth exploration of the optical characteristics of nanomaterials, fluorescent nanomaterials, a class of nanoscale materials that can absorb light radiation at specific wavelengths and emit fluorescence at different wavelengths, have attracted the interest of researchers and have gradually become a research hotspot.[1–3] Compared with traditional fluorescent molecules, fluorescent nanomaterials exhibit both size and fluorescence characteristics. They not only have excellent photostability, high quantum yield, and adjustable emission wavelength,[4,5] but can also achieve adequate biocompatibility and targeting capability through surface modification.[6,7] These unique advantages show great application potential in the fields of biological imaging,[8,9] disease diagnosis,[10,11] photoelectric devices,[12,13] and sensing detection,[2,14] as well as in the research and application of nanomaterials, from basic performance exploration to new stages of functionalization and precision.[15]

Among the currently available fluorescent nanomaterials, the most common class comprises downshifting luminescent materials, including semiconductor quantum dots, small-molecule dyes, organic modified silica, and gold nanoparticles.[6,16,17] These materials follow the energy conversion law of "high-energy short-wavelength light input-low-energy long-wavelength light output." Although downshifting fluorescent materials occupy an important position owing to their advantages of a relatively mature synthesis process and wide adjustable range of emission spectra, their inherent defects are gradually emerging in high-end applications. For instance, the heavy metal ions of quantum dots (such as cadmium and lead) can easily cause biological toxicity,[18] the photobleaching characteristics of organic dyes limit long-term dynamic monitoring,[19] furthermore, when ultraviolet or visible light is used as the excitation source, the resulting strong tissue absorption and scattering limit the tissue penetration depth to less than 1 cm and cause significant autofluorescence, interfering with observation.[20] Moreover, it is difficult to meet key research needs such as deep-tissue imaging and long-term tracking *in vivo*, as strong light irradiation can cause light damage to biological tissues.[21]

It should be noted that over the past decade, researchers have successfully overcome some limitations of traditional UV/

[a]*College of Life Sciences, Shihezi University, Xinjiang Production and Construction Corps Key Laboratory of Oasis Town and Mountain-basin System Ecology, Key Laboratory of Xinjiang Phytomedicine Resource Utilization, Ministry of Education, China. E-mail: shifeng2314@yeah.net*

[b]*Kuitun Traditional Chinese Medicine Hospital of Xinjiang Production and Construction, Kuitun, 833200, China. E-mail: jhdys@sina.com*

† Equal contribution.

visible light excitation by developing downshifting probes that are excited in the first near-infrared window (NIR-I, 680–950 nm) and emit in the second near-infrared window (NIR-II, 1050–1350 nm), significantly improving the penetration depth and signal-to-noise ratio for *in vivo* imaging. This strategy has been highly successful in minimizing absorption, scattering, and autofluorescence, and the underlying physical mechanism typically features a higher quantum yield than the upconversion process.[22]

In this context, the emergence of rare earth upconversion nanomaterials (UCNPs) has provided another important approach to overcoming the limitations of traditional fluorescent materials.[23,24] The discrete 4f energy levels and low phonon energies of rare-earth ions (*e.g.*, Yb^{3+}, Er^{3+}, Tm^{3+}) make them ideal for upconversion. However, the optical absorption *via* f–f transitions is inherently weak owing to their forbidden nature, governed primarily by the Laporte parity rule ($\Delta l = 0$) with additional constraints from the spin selection rule. This low absorption efficiency constituted a key limiting factor in their initial applications.[25] These nanoscale light-emitting materials doped with rare earth elements (such as Yb^{3+}, Er^{3+}, and Tm^{3+}) can directly convert low-energy NIR long-wavelength light (such as 980 nm and 808 nm) into high-energy visible/ultraviolet short-wavelength light through a unique multi-photon energy conversion mechanism. This anti-Stokes luminescence phenomenon breaks the energy conversion law of traditional fluorescent materials. In particular, near-infrared light exhibits minimal scattering and weak absorption in biological tissues, and the background of biological autofluorescence is extremely low. Combined with their excellent photostability and millisecond-long fluorescence lifetime, UCNPs are promising for bioimaging applications. Their key features—deep-tissue penetration of NIR excitation light and minimal autofluorescence—enable long-term dynamic monitoring with low background interference, despite the challenge of tissue attenuation for the upconverted visible light. This unique combination has brought about subversive potential in biomedicine, energy optics, information storage, and other fields.[23,26]

The history of upconversion luminescence research represents breakthroughs in scientific exploration. In 1959, Soviet physicist Nikolai Basov first predicted the possibility of multi-photon absorption to theoretically achieve anti-Stokes luminescence.[27] In 1966, Canadian scientist Frank Auzel experimentally observed visible light emission excited by infrared light in Er^{3+}–CaF_2 (calcium fluoride) glass for the first time and proposed the excited-state absorption (ESA) mechanism, which marked the official beginning of upconversion luminescence research.[28] In 1970, Auzel formally proposed the term "upconversion" to systematically clarify the physical nature of this luminescence process.[29] In the 1980s, the discovery of the energy transfer upconversion (ETU) mechanism and the development of low-phonon energy matrix materials such as $NaYF_4$ led to a qualitative leap in upconversion efficiency—revealing that the efficiency of hexagonal β-$NaYF_4$ is 5 to 10 times that of the cubic phase.[30] In the 21st century, breakthroughs in nanotechnology have enabled the controlled synthesis of UCNPs.[31] Improvements in the size uniformity and surface modifiability allowed UCNPs to accurately adapt to the *in vivo* environment, and their unique advantages in biomedical imaging, photodynamic therapy, and other fields have rapidly triggered a global research upsurge.

However, the large-scale application of UCNPs still faces multiple challenges that must be overcome. At the preparation level, after performing existing synthesis technologies such as high-temperature pyrolysis and the hydrothermal method, it may still be challenging to jointly regulate the size uniformity (the polydispersion index [PDI] is often >0.1), crystal structural integrity, and surface modification of nanomaterials.[24] In addition, the technical barriers of high purification costs and precise control of the doping ratio of rare earth elements lead to the poor repeatability of large-scale preparations, seriously restricting industrialization. In terms of performance optimization, the quantum yield of multi-photon transitions is generally low (usually <5%), the excitation optical power density is high (often >1 W cm^{-2}), the luminous wavelength is limited by the inherent energy level structure of rare-earth ions, and the ability for full-spectrum control remains insufficient.[32,33] Overcoming the bottleneck in luminous efficiency has become a primary issue that restricts its practical application. At the biomedical transformation level, surface ligands are easily shed in the physiological environment and cause particle agglomeration.[34] Moreover, the long-term *in vivo* metabolic pathways involved and their biocompatibility remain to be elucidated, the efficiency of targeted modification leads to off-target effects, and strong light excitation may cause local thermal effects (temperature rise >2 °C).[35] These problems pose challenges regarding the safety of UCNPs in *in vivo* applications.

In light of these developments and remaining drawbacks, this review summarizes the basic characteristics and application breakthroughs of UCNPs. First, the core concepts and luminescence mechanisms of the UCNPs are briefly summarized. This paper focused on key strategies to enhance luminous efficiency, including core–shell structure optimization, lattice engineering, surface functionalization, and other frontier technologies. This paper also systematically reviewed the latest research progress on UCNPs in the biomedical field in recent years, especially breakthrough applications in deep-tissue high-resolution imaging, high-sensitivity biosensing, and precision photodynamic therapy. Finally, the developmental direction of UCNPs in material design innovation and clinical translation was proposed to provide a reference for promoting the development of UCNPs from laboratory research to practical applications.

2. Basic characteristics of UCNPs

2.1. The composition of UCNPs

It is well known that UCNPs are usually composed of three parts: a matrix, an activator, and a sensitizer.[36] The activator is the luminescence center of the UCNPs, while the sensitizer enhances the luminescence effect by absorbing and transferring energy. Although the matrix is not directly involved in the luminescence process, it provides the necessary carrier environment for the activator.[37,38]

2.1.1. Dopant: central to luminescence performance. Doping with lanthanide ions is central to tailoring the luminescence properties of UCNPs. The excitation wavelength, emission spectrum, and quantum efficiency can be accurately controlled by designing the type, concentration, and combination of the rare earth (RE) ions. They can be divided into two categories based on their functions: sensitizers and activators. Sensitizers absorb excitation light and transfer energy. For example, Yb^{3+}, which has a simple two-level structure and large absorption cross-section, can efficiently absorb near-infrared light and deliver it to the activator.[39] In addition, using Yb^{3+} as a sensitizer can significantly improve the upconversion efficiency, especially when co-doped with Er^{3+}, Tm^{3+}, or other activators. Meanwhile, the activator, which is responsible for receiving the realized characteristic emission from the sensitizer, such as Er^{3+}, Tm^{3+}, Ho^{3+}, has a long excited-state lifetime and can achieve efficient upconversion luminescence. The choice of activator determines the color and efficiency of the upconversion luminescence. For example, Er^{3+} emits green and red light upon excitation at 980 nm, whereas Tm^{3+} emits blue light upon excitation at 808 nm.[40]

It should be clarified that while the above classification applies to energy transfer upconversion, in systems where upconversion occurs through Ground State Absorption (GSA) with single ion doping, the same dopant RE^{3+} ions can simultaneously play both sensitizer and activator roles.[41]

2.1.2. Matrix: key to non-radiative transition rates. The matrix serves to govern the non-radiative transition rate in UCNP systems. The matrix material itself does not emit light and is therefore an optically inert component. It significantly affects the quantum efficiency and spectral properties of the upconversion process by providing a low-phonon energy environment, optimizing the crystal field symmetry, and regulating the energy transfer efficiency between rare earth ions. Its central role is to provide a suitable crystal field for ion activation. An ideal matrix should exhibit high chemical stability, low phonon energy, good lattice matching with rare earth ions, and low absorption of incident light.[42] The requirement for low phonon energy stems from the energy gap law in photophysics: a lower phonon energy increases the number of phonons required to bridge the energy gap between electronic states, thereby exponentially reducing the non-radiative decay rate and enhancing radiative emission. They are mainly divided into various categories according to their chemical composition:[43] (1) fluorides (*e.g.*, $NaYF_4$ and $NaGdF_4$) are the most widely used matrices. They have extremely low phonon energy (<400 cm^{-1}) and high chemical stability, which can effectively suppress non-radiative transitions and significantly improve the upconversion efficiency. The efficiency of hexagonal β-$NaYF_4$ was found to be 5–10 times higher than that of the cubic phase due to its excellent symmetry and low non-radiative transition rate.[44] Similarly, the energy transfer efficiency of Yb^{3+}–Er^{3+} is also approximately three times higher in the hexagonal phase than in the cubic phase;[45] (2) oxides (*e.g.*, Y_2O_3 and Gd_2O_3) are widely used in biological detection due to their high chemical stability, good biocompatibility, and easy synthesis. However, their high phonon energy (>600 cm^{-1}) limits their upconversion efficiency;[46] (3) fluorine oxides (*e.g.*, YOF and LaOF) combine the low phonon energy of fluoride with the high stability of oxides. This material can be optimized by precisely adjusting the fluorine/oxygen ratio;[47,48] (4) sulfides (such as La_2S_3) have intermediate phonon energy (~400–500 cm^{-1}) and unique optical properties.[49] For instance, it can weakly absorb infrared light (especially long wavelengths, such as 1550 nm), which is suitable for upconversion applications for the corresponding wavelength;[50] (5) organic–inorganic hybrid matrices: beyond conventional inorganic matrices, rare-earth-doped organic–inorganic hybrid materials have attracted considerable attention. Among these, the group led by Luis Carlos[51] has made outstanding contributions, developing a series of hybrid matrices with excellent luminescence properties and tunable characteristics, which have significantly expanded the application prospects of upconversion materials in optoelectronic devices. (6) Metal–organic frameworks (MOFs):As emerging matrices, the porous structures and designability of MOFs[52] offer the possibility of multi-functional integration, such as ZIF-8-coated UCNPs, which have both fluorescence and drug-loading capabilities.[53]

2.2. The luminescence mechanism of UCNPs

The luminescence mechanism of UCNPs is based on the unique electronic structure of rare earth ions and a multistage energy transfer process, which achieves anti-Stokes luminescence by absorbing multiple low-energy photons and emitting high-energy photons. This process involves complex energy level transitions and energy transfer pathways, the main mechanisms of which can be divided into the following categories: excited-state absorption (ESA), energy transfer upconversion (ETU), cross-relaxation (CR), photon avalanche (PA), and cooperative sensitization upconversion (CSU)[54,55](Fig. 1).

2.2.1. ESA. ESA occurs inside a single activator ion, which absorbs a second photon that jumps to a higher energy level when the metastable state is not relaxed and then emits high-energy photons. This mechanism is particularly important in the upconversion process because it can realize photon transition from low to high energy to improve the luminescence efficiency of the material. However, this process requires a high excitation power; this energy level structure often occurs in rare earth ions, especially Er^{3+}, Yb^{3+}, and Nd^{3+}. In the upconversion process, ESA affects the luminescence intensity and the wavelength and lifetime of luminescence.[56] For example, in Nd^{3+}-doped $Y_3A_{l5}O_{12}$, $YLiF_4$, and $LaMgAl_{11}O_{19}$ crystals, experimental results show that ESA is important for laser operation, especially in the case of flash pumps. Furthermore, the Judd–Ofelt theory provides a clear description of ESA.[57] However, upconversion energy transfer losses are also important because they may limit the storage capacity at high excitation pump powers.[58]

2.2.2. ETU. ETU is the most common and efficient mechanism.[59] It involves the synergistic action of the sensitizer and activator, which absorbs photons and then transfers energy to the neighboring activator. Finally, the activator relaxes and emits upconversion light. The mechanism is efficient and can

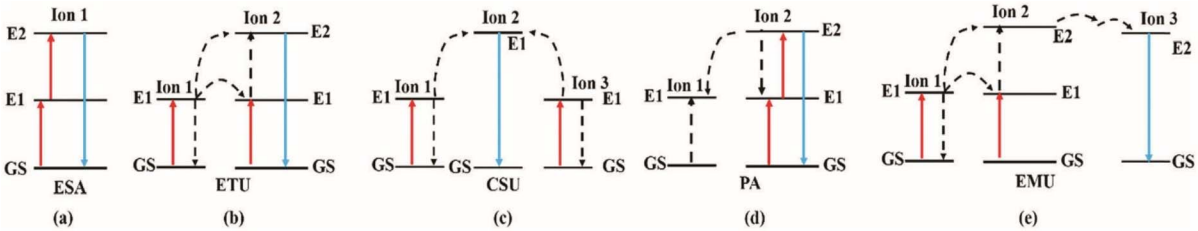

Fig. 1 Ln-doped UCNPs. GS: ground state; E1 and E2: excited states; (a) ESA: excited-state absorption; (b) ETU: energy transfer upconversion; (c) CSU: cooperative sensitization upconversion; (d) PA: photon avalanche; (e) EMU: energy migration upconversion.[55] This figure is reproduced from ref. 55 with permission from The Royal Society of Chemistry C. Duan, L. Liang, L. Li, R. Zhang and Z. Xu, *Journal of Materials Chemistry*. B, 2018, **62**, 192–209, Copyright 2025.

operate at low power but requires that the ions be sufficiently close to each other. Yb^{3+} is an ideal sensitizer for ETU due to its high absorption cross-section at 980 nm.[60,61] By absorbing NIR light and transferring the energy to the activator, Yb^{3+} can achieve efficient upconversion luminescence. The upconversion system of Yb^{3+} as a sensitizer was first reported in 1966 by the American scientist Frank Auzel. He found that the green light emission intensity at 980 nm was significantly enhanced in fluoride crystals co-doped with Yb^{3+} and Er^{3+}.

2.2.3. CR. CR is a non-negligible interionic interaction during the upconversion process. However, this process is concentration dependent. At high doping concentrations, the inter-ion distance decreases and the probability of CR increases significantly, which may lead to concentration quenching.[62] However, if CR can be precisely regulated, light color and space-time regulation of upconversion luminescence can be realized, which has important application value in many fields.[63] For example, by adjusting the doping concentration of Tm^{3+} ions, Professor Zhou Bo's team[64] achieved precise control of the CR process and, thus, a tunable light color.

2.2.4. PA. PA has a unique and highly efficient mechanism of action. When a small number of ions reach a specific "bottleneck" intermediate state, they rapidly absorb photons to a high energy level due to their huge absorption cross-section and transfer energy to the ground state ions through CR, triggering an avalanche-like accumulation of particle numbers and intense luminescence.[65] In other words, PAs have a higher nonlinear response and higher luminescence efficiency than other upconversion mechanisms (such as ESA, ETU, and CSU). For instance, ESA typically occurs in samples with low doping concentrations because the ions are isolated from each other, which limits other types of upconversion. ETU involves energy transfer between two adjacent ions, which is less efficient but helps achieve high-resolution imaging. PAs have broad application prospects in multiple fields, including biological imaging, super-resolution microscopic imaging, and infrared quantum counting. For instance, by adjusting the Gd^{3+}-assisted energy transfer, the emission wavelength tuning of Tm^{3+}-sensitized PA nanoparticles (ANPs) can be achieved, generating highly nonlinear emissions of Eu^{3+}, Tb^{3+}, Ho^{3+}, and Er^{3+} ions.[66,67] Recently, a key breakthrough in realizing this mechanism at the nanoscale was achieved by Skripka *et al.*[68], who clearly observed and optimized the photon avalanche process within individual UCNPs through meticulously designed core–shell structures, laying the foundation for ultra-sensitive detection and super-resolution imaging. In addition, PAs can be extended to combinations with other fluorescent molecules such as CdS/CdSe/CdS core–shell quantum dots, thereby achieving a wider range of photon applications.[69]

2.2.5. CSU. The core feature of CSU is that two or more sensitizer ions simultaneously transfer energy to one activator ion, thereby achieving efficient anti-Stokes luminescence. Compared with the traditional single-sensitizer system, the CSU can overcome the limitation of single-ion energy transfer and generate unique luminescent properties under excitation at specific wavelengths.[70] In 2024, Professor Sun Lining's team[71] designed an upconversion luminescent eutectic aggregate with a mononuclear Yb^{3+} complex as the sensitizer and a mononuclear Eu^{3+} complex as the activator. Under excitation with 980 nm NIR light, the Yb^{3+}-Yb^{3+} ion pair absorbed photons and then transferred them to the Eu^{3+} ion in a synergistic sensitization upconversion manner, achieving the red upconversion luminescence of Eu^{3+}. Meanwhile, under excitation with 365 nm ultraviolet light, it can also obtain the red downshifting luminescence of Eu^{3+} ions. They further explored the influence of different proportions and molecular combinations on luminescence. When the molar ratio of Yb^{3+} : Eu^{3+} was 1 : 1, the luminescence intensity was strongest. Under 980 nm light excitation (2.1 W cm^{-2}), it exhibits an upconversion luminescence quantum yield of 0.67 ± 0.03%, which is approximately 100 times higher than that of the Yb/Tb ion pair at the same molecular level.

2.3. The preparation method of UCNPs

There are various methods for preparing UCNPs, all of which have the core goal of obtaining nanoparticles with a controllable size, uniform morphology, high crystallinity, and high luminous efficiency.[72] The most commonly used synthesis methods include co-precipitation, the sol–gel method, the water/solvothermal method, and thermal decomposition.

2.3.1. Co-precipitation method. The co-precipitation method produces a solid product upon the action of a precipitant and more than two types of metal salt solutions after co-precipitation. Several components can precipitate simultaneously, and the distribution between them is relatively uniform. This was an early and commonly used method that is inexpensive and simple to perform, and the size of the product

can be adjusted.[73,74] A study by Girardet, T. *et al.*[75] showed that upconversion nanocrystals of a $NaYF_4$ matrix can be synthesized *via* co-precipitation, and a core–shell structure can be formed by introducing precursors. This one-pot method of continuous layer-by-layer coating not only simplifies the synthesis step but also improves the synthesis efficiency and enables the precise regulation of shell thickness. However, the traditional co-precipitation method produces a large number of defects on the surface of nanocrystalline products with heterogeneous sizes, resulting in luminescence quenching. Particles produced in this manner are suitable for applications with low requirements for luminescence efficiency and particle size uniformity or for basic research.[76,77]

Owing to its simplicity and flexibility, co-precipitation remains the mainstream method for preparing UCNPs. Researchers are gradually overcoming the shortcomings associated with this method. The modified co-precipitation method includes the microwave-assisted water phase co-precipitation method, which can significantly improve the reaction rate, promote the formation of uniform particles, and enhance the crystallization performance of the product. It has been reported that microwave heating can accelerate the growth of MIL-53(Al) crystals and increase their crystallinity and size when they are synthesized using the microwave-assisted hydrothermal method.[78,79] Similarly, in the preparation of iron oxide nanoparticles *via* microwave-assisted co-precipitation, microwaves can improve the dispersibility and monodispersibility of particles, making them more suitable for biomedical applications.[80]

2.3.2. Sol–gel method. The sol–gel method is the most important wet chemical method for the synthesis of UCNPs.[81,82] It is based on the formation of gels through the polycondensation and hydrolysis of metal–organic matter or inorganic salts as matrix, followed by sintering to produce UCNPs. Although sol–gel synthesis provides excellent compositional control and high-temperature stability, it provides poor control of the particle size and phase purity. Recently, researchers have overcome these shortcomings by improving the sol–gel method. The microwave-assisted sol–gel method has become a research hotspot in the field of materials science due to its significant improvement in synthesis efficiency and material properties. Compared with traditional sol–gel methods, the microwave-assisted method significantly shortens the reaction time, reduces the crystallization temperature, and can obtain more uniform and smaller-sized nanoparticles.[83,84]

2.3.3. Hydrothermal method. The hydrothermal method is a cost-effective and environmentally sound alternative that can be performed under high temperatures and pressures inside a sealed autoclave.[85,86] This method of preparing materials involves the use of water as a solvent, and the rare earth and other powder is dissolved and recrystallized in a sealed pressure vessel. Compared to other the preparation methods, the powder obtained using the hydrothermal method has the advantages of complete grain development, small particle size, uniform distribution, light particle agglomeration, cheaper raw materials, and ease of obtaining the appropriate stoichiometry and crystal form. Different morphologies, such as nanorods, nanoflowers, and core–shell structures, can be realized by adjusting the reaction parameters.[87] Therefore, water/solvothermal methods have become the mainstream method for preparing high-performance UCNPs owing to their precise crystalline phase formation and morphology control capabilities.

2.3.4. Thermal decomposition method. Decomposition at 300 °C with a high-boiling-point organic solvent such as 1-octadecene is the basis for thermal decomposition synthesis using organometallic trifluoroacetate as a precursor.[88] Yan *et al.*[89] reported the synthesis of triangular LaF3 nanoplates with a size of 2.0 × 16.0 nm using oleic acid and octadecene solutions in the presence of $La(CF_3COO)_3$ *via* thermal decomposition. Subsequently, Yan and his team further improved their method to obtain high-quality cubic phase (α phase) and hexagonal phase (β phase) NaREF4 (RE: Pr to Lu or Y) nanocrystals (nanopolyhedrons, nanorods, nanosheets, and nanospheres) and NaYF4:Yb,Er/Tm nanocrystals (nanopolyhedrons and nanosheets).

Thermal decomposition has become the preferred method for preparing high-performance UCNPs owing to its ability to provide excellent size control and crystalline phase purity. However, thermal decomposition has certain shortcomings that cannot be ignored.[90,91] For example, the reaction conditions must ensure that no oxygen is present, *i.e.*, the reaction must be carried out under an inert gas atmosphere, which complicates the operation. In addition, thermal decomposition may produce toxic gases during preparation. Finally, organic solvents are used in this process, which can increase production costs.

Today, this process is actively moving toward the development of greener and safer alternatives. For example, Liang *et al.*[92] developed a modified microwave-assisted thermal decomposition method to rapidly produce monodisperse Fe_3O_4 nanoparticles at a lower aging temperature. This method not only improved the yield but also successfully fabricated superparamagnetic Fe_3O_4 nanomaterials with specific shapes, such as quadrilateral, hexagonal, rod-shaped, and triangular morphologies.

3. Optical properties of UCNPs

As a new type of labeling material, UCNPs have become key candidates for overcoming the bottleneck of existing optical technologies because of their NIR-range excitation, narrow band emission, long fluorescence lifetime, excellent photostability, and absence of background autofluorescence interference.[93–95] However, the low luminescence efficiency of UCNPs, especially the inherent weak absorption cross-section of rare earth ions, long multi-phonon relaxation, and unavoidable surface quenching effect at the nanoscale, constitute the biggest obstacles for their wide application.[96,97] Therefore, it is of great research value and urgency to explore and systematically solve the root causes of low upconversion luminescence efficiency and develop efficient, stable, and controllable UCNP systems.

Before delving into the detailed discussion of the optical properties of upconversion nanoparticles, it is crucial to clearly define the key metric frequently used in this study—quantum

yield (QY). The QY is a core parameter for measuring luminescence efficiency and must be distinguished as follows:

(1) The external quantum yield (EQY) refers to the number of emitted photons per incident photon, reflecting the overall system efficiency from the excitation source to the final luminescence.

(2) The internal quantum yield (IQY) refers to the number of emitted photons per absorbed photon, directly characterizing the intrinsic efficiency of the material itself in converting absorbed energy into radiative energy.

Owing to the multiphoton absorption involved in the upconversion process, its IQY is typically much lower than that of conventional downshifting materials. Furthermore, the EQY is additionally limited by factors such as nanoparticle scattering, reflection, and absorption cross-section.[98] Unless otherwise specified, the subsequent discussions in this review refer to the IQY.

3.1. Material design

Surface chemistry is a key factor in regulating the performance and biocompatibility of UCNPs. Hemmer's team[99] systematically studied the effects of different ligands and coatings on the luminescence efficiency, colloidal stability, and cellular uptake behavior of UCNPs, providing important guidance for the design of high-performance bioprobes. Material design is the core link to improve the luminescence performance of UCNPs. At present, UCNP research mainly focuses on four key directions: core–shell structure optimization,[37,100] lattice engineering,[101,102] surface modification,[36] and the identification[36] and development of new matrix (Fig. 3).[103]

In terms of core–shell structure optimization, the $LiYF_4$@-$LiErF_4$@$LiYF_4$ (Y@Er@Y) nanocrystals designed by Fujian Institute of Materials Engineering adopted a "sandwich structure," where their inert shell coating effectively suppressed the energy dissipation caused by surface defects.[104] (Fig. 2). Using the method, the upconversion luminescence intensity of Er^{3+} increased 760-fold, and the quantum yield was significantly increased from <0.01% to 2.29% upon the introduction of Tm^{3+} as the energy capture center. At a low temperature (77 K), the energy transfer rate of the material was reduced by a factor of 10, and the luminescence intensity was further enhanced 27.7-fold, marking an important breakthrough in enhancing luminescence efficiency (Fig. 2). At the same time, the precise regulation of the core–shell structure has also achieved remarkable results. By adjusting the shell thickness, ion

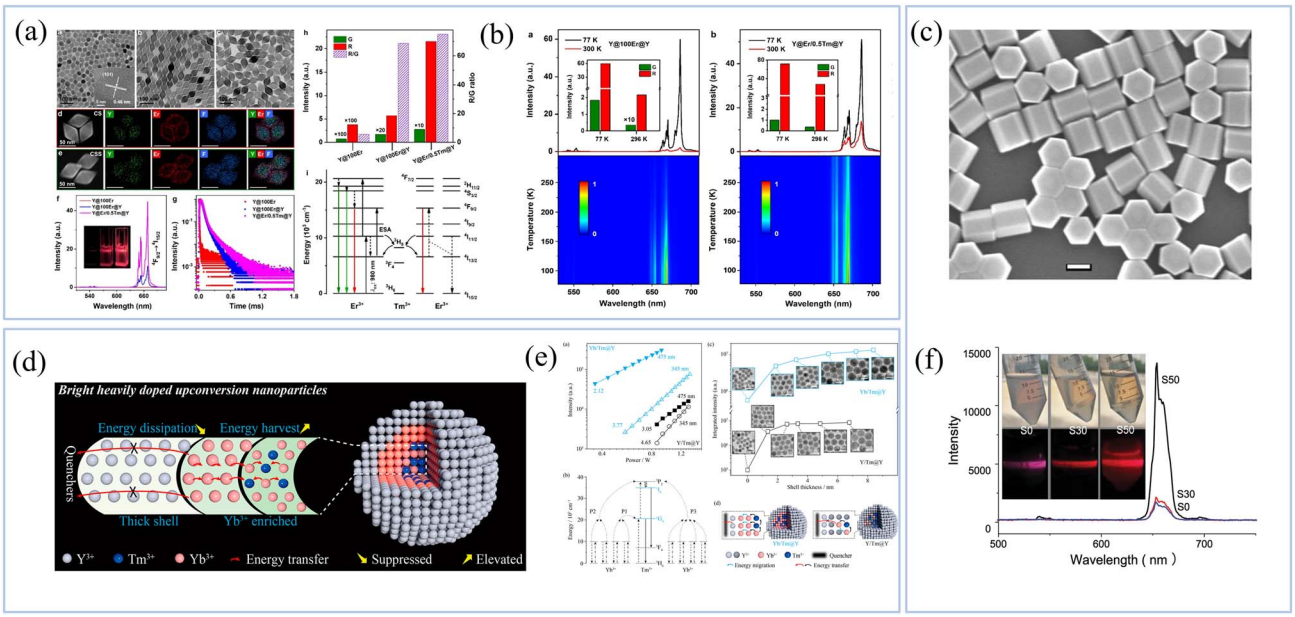

Fig. 2 (a) TEM images of (a) $LiYF_4$ core-only, (b) Y@100Er CS, and (c) Y@100Er@Y CSS UCNPs. The insets show the corresponding UCL photographs of UCNPs dispersed in cyclohexane (1 mg mL^{-1}). The corresponding UCL decay curves from $^4F_{9/2}$ ($\lambda_{em} = 668$ nm) of Er^{3+} in UCNPs shown in (f). (b) UCL spectra of (a) Y@100Er@Y and (b) Y@Er/0.5Tm@Y UCNPs at 77 and 300 K, upon 980 nm excitation with a power density of 20 W cm^{-2}. The insets show the integrated UCL intensities for the green and red emissions of Er^{3+}. The bottom patterns show the contour plots of the temperature-dependent UCL spectra. (c) Morphological evolution of S50 at 220 °C (d) energy control mechanism of high brightness heavily doped upconversion nanoparticles (e) upconversion emission intensity of Yb/Tm@Y and Y/Tm@Y at ~345 and 475 nm *versus* the excitation power; (3) upconversion luminescence intensity (integrated from 250 to 850 nm) of Yb/Tm@Y and Y/Tm@Y UCNPs with different NaYF4 shell thicknesses (4) schematic illustration of the energy transfer from the emitting core to surface quenchers in Yb/Tm@Y and Y/Tm@Y UCNPs. (f) UCPL spectra of the sol (0.5% in water) containing β-NaErF4:Yb doped with different amount of Ca^{2+}. Inset shows the photographs of the corresponding samples under daylight (top) and 980 nm laser irradiation.[104,105,112] Figure description, adapted/reproduced from ref. 104, 105, 112 with permission from ACS Publications S. Zhang, X. Hu, P. Huang, X. Shang, D. Yang, Z. Shao, X. Wang, W. Zheng and X. Chen, *Nano Letters*, 2025, **25**, 7426–7434. & ScienceDirect Y. Niu, Z. Bao, Y. Gao, M. Guo, J. Liu, J. Shao, M. Lu, Z. Yuan and X. Xie, *Journal of Rare Earths*, 2023, https://doi.org/10.1016/j.jre.2023.02.022 & ACS *Applied Materials & Interfaces* X. Qin, J. Liu, Y. Xu, B. Li, J. Cheng, X. Wu, J. Zhang, Z. Liu, R. Ning and Y. Li, *ACS Applied Materials & Interfaces*, 2020, **12**, 31225–31234, Copyright 2025.

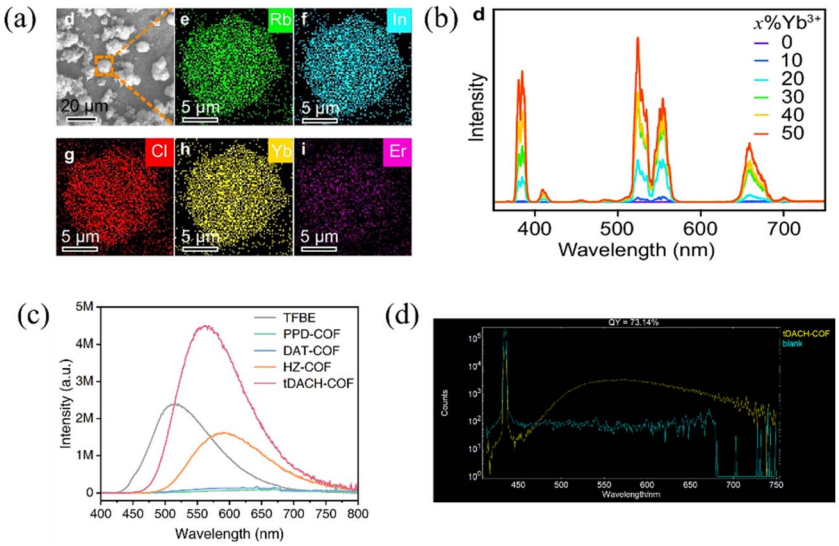

Fig. 3 (a) EDS elemental mappings (Rb, In, Cl, Yb, and Er) of Rb_3InCl_6: 50%Yb^{3+}/4%Er^{3+} MCs. (b) UCL spectra of Rb_3InCl_6: *x*%Yb^{3+}/1%Er^{3+} MCs with different Yb^{3+} concentrations under 980-nm excitation at a power density of 60 W cm^{-2} (c) photoluminescence spectra of tDACH-COF, HZ-COF, PPD-COF, and DAT-COF, and TFBE powders. (d) Screenshot of the instrument used for the quantum yield testing of tDACH-COF.[115,116] Figure description, reproduced from ref. 115 and 116 with permission from *Nature Communications* W. Zhang, W. Zheng, P. Huang, D. Yang, Z. Shao, W. Zhang, H. Zhang, Z. Xie, J. Xu and X. Chen, *Nature Communications*, 2025, **16**, 6762 & Cell Press L. Liang, J. Li, J. Ning, Y. Wang, B. Zu and X. Dou, *Cell Reports Physical Science*, 2025, **6**, Copyright 2025.

distribution, and multi-layer heterojunction structure, surface quenching can be effectively suppressed and energy transfer efficiency can be enhanced, thereby significantly improving the upconversion luminescence intensity and enabling precise regulation of the emission color. For instance, thick inert shells can substantially reduce surface quenching and improve the luminescence efficiency of heavily doped nanoparticles, while multi-layered core–shell structures and multi-heterojunction designs facilitate bidirectional energy transfer and multicolor emission, with red light enhancement reaching up to hundreds of times[105] (Fig. 2).

In addition to core–shell structure optimization, the degree of matching of dopants and matrix in lattice engineering is crucial for regulating luminescence performance. When the radius of rare earth ions is significantly different from that of the cation in the matrix lattice, it can easily cause lattice distortion and form defect centers, which in turn become energy-quenching channels.[106–108] Specifically, when Yb^{3+} (ionic radius = 0.868 Å) was selected as the sensitizer in the $NaYF_4$ matrix, its radius was close to that of Y^{3+} (0.893 Å), resulting in high lattice matching and little energy transfer loss. However, when an ion with a large radius difference is selected, such as La^{3+} (1.032 Å), the upconversion efficiency decreases by more than 30% due to lattice distortion.[109]

On this basis, the lattice field regulation initiated by doped ions can effectively enhance luminescence performance.[110,111] For instance, Yu *et al.*[112] reported that adding 50 mol% Ca^{2+} ions to β-$NaErF_4$:Yb nanocrystals could reduce the local crystal field symmetry around the activator ions, break the 4f–4f barrier transition of Er^{3+}, and increase red upconversion luminescence intensity 8-fold (Fig. 2). Xie *et al.*[113] also found that after doping 25 mol% Gd^{3+} ions into $NaErF_4$:Yb nanocrystals, the crystal field distortion caused by the difference in ionic radii could increase the probability of the electric dipole transition of Er^{3+}, thereby enhancing the upconversion luminescence intensity. Similarly, when In_2O_3 is doped with high-valency Al^{3+}, the intensity of the emission peaks near 552 nm and 661 nm of Er^{3+}/Yb^{3+} phosphor significantly increases upon excitation with a 980-nm laser; the luminous intensity reaches a maximum when doped with 2% Al^{3+} ions.[114] This is due to the lattice contraction caused by the substitution of the large-radius In^{3+} by Al^{3+}, which breaks the local symmetry; this enhances the probability of the f–f transition.

In addition, the limited energy transfer strategy of zero-dimensional materials provides new ideas for performance improvement.Zhang *et al.*[115] proposed this strategy. By designing an Yb^{3+}/Er^{3+} co-doped Rb_3InCl_6 crystal, the Er^{3+} breakthrough was successfully achieved at 384 nm UV upconversion emission, with an intensity ratio (I_{384}/I_{554}) of 0.864. This is 1–2 orders of magnitude higher than that of traditional materials and has been applied to the remote photocontrolled modification of perovskite nanocrystals (Fig. 3).

Finally, when developing novel matrix, the application of covalent organic frameworks (COFs) provides new ideas for performance breakthroughs. Liang *et al.*[116] achieved a quantum confinement effect in COFs and 73% photoluminescence quantum yield through molecular design without reducing the physical size of the material. The TTDACH-COF material also performs well in the sensing field, with a detection limit as low as 4.6 ppb for nerve agent mimetics (Fig. 3).

3.2. Energy transfer regulation

Energy transfer regulation is the core breakthrough in UCNP performance optimization. In recent years, research teams have

made several important discoveries regarding the innovation of energy transfer paths,[117] co-doping strategies,[118,119] and the development of new sensitizers[120]

In the innovative exploration of energy transfer paths, the team led by Gan Zongsong from the Huazhong University of Science and Technology[121] proposed a "rare earth upconversion + three-wire upconversion" cascade mechanism, in which the 11-nm rare earth core–shell nanoparticles they prepared achieved high-concentration monodisperse photoresist doping. Through energy level coupling, the energy from the rare earth core is locally transferred to the molecular triplet state, increasing the upconversion efficiency to the threshold that triggers the lithography reaction. Thus, Zongsong and colleagues successfully achieved NIR four-photon lithography with a resolution comparable to that of femtosecond-laser two-photon lithography.

Aside from the construction of new energy transfer paths, multi-ion co-doping has been an important research direction for UCNPs in recent years. Zhang *et al.*[122] designed quadruple-doped (Nd^{3+}, Tm^{3+}, Er^{3+}, and Yb^{3+}) core–shell structured $NaYF_4$ upconversion nanoparticles (UCNPs) to achieve multicolor luminescence from a single material. Specifically, they constructed a multi-layer nanostructure—$NaYF_4$: 30% Yb^{3+}, 0.1% Er^{3+}, 0.9% Tm^{3+}, 5% Nd^{3+} @ $NaYF_4$: 30% Yb^{3+}, 0.5% Tm^{3+} @ $NaYF_4$—that exhibits white light emission under 980 nm laser excitation. The corresponding CIE coordinates shift from (0.356, 0.335) to (0.333, 0.317) as the excitation power increases from 0.2 W to 1 W, falling within the standard white light region defined by the CIE. Moreover, by adjusting the doping concentrations of the activator ions (Er^{3+} and Tm^{3+}), the structure can achieve multicolor emission spanning red, green, cyan, blue, and white. This tunability originates from a dynamic energy transfer process responsive to changes in excitation power or wavelength. Such a rare-earth co-doped core–shell architecture offers a novel strategy for achieving multicolor luminescence within a single $NaYF_4$ system. It not only provides a new pathway for tunable steady-state full-color emission but also exhibits unique optical properties, making it promising for security anti-counterfeiting applications.

This leads to the third, and crucial, direction in energy transfer regulation—the development of new sensitizers to overcome the limitations of conventional excitation. Although Yb^{3+} is the most efficient sensitizer, its optimal excitation wavelength of 980 nm coincides with the strong absorption band of water molecules, which can cause significant local thermal effects in bio-applications, limiting imaging depth and potentially causing tissue damage. Therefore, finding alternative sensitizers has become a major research focus in the field. Among them, Nd^{3+}, with its strong absorption peak around 800 nm—a wavelength at which water exhibits extremely low absorption—has emerged as the most prominent candidate to replace Yb^{3+}, laying the foundation for deep-tissue, low-photothermal imaging.[123] Additionally, exploration of other ions, such as Cr^{3+}, has opened new avenues for expanding the excitation wavelength range to 800–900 nm, with applications already achieving *in vivo* imaging penetration depths exceeding 3 cm.[124]

These innovative designs centered on energy transfer regulation—from the construction of cascade mechanisms, optimization of collaborative doping, and the development of new sensitizers—and have jointly driven the breakthrough applications of UCNPs in multiple fields. For instance, in the biomedical field, the signal-to-noise ratio of deep-tissue imaging upon excitation with an 808-nm laser has reached 28 : 1;[37,125] in the energy sector, it has helped increase the efficiency of solar cells by 4.3%;[126,127] in the field of information storage, a 5D optical storage density of 10^{12} bit cm^{-3} was achieved.[128,129]

3.3. Non-radiative transitions

Among the key factors that restrict the efficiency and stability of UCNPs, non-radiative transitions caused by surface defects and lattice vibration are particularly prominent.[130] To address this core challenge, researchers have focused on surface modification and defect regulation strategies and have effectively improved the luminescence performance and environmental adaptability of materials through precise design.[131,132]

A team from Hebei University[133] developed an innovative organic ligand coating strategy by building an organic-inorganic hybrid layer on the surface of nanocrystals to form an efficient energy protection barrier. The core mechanism is reflected in two aspects. First, the organic ligand passivates the surface hanging bond through coordination, which directly inhibits the energy quenching caused by surface defects. Second, the low vibrational frequency characteristics of the organic phase can effectively decouple the high-energy vibrations of the matrix lattice, such as the high-frequency vibrations of O–H and C–H bonds, and reduce the vibration-induced non-radiative transition losses. Experimental data has shown that the luminescence intensity of the materials modified using this strategy is not only increased by three orders of magnitude at room temperature, but also enhanced by six orders of magnitude in the high-temperature environment of 443 K (approximately 170 °C), which breaks through the technical bottleneck of the poor stability of traditional UCNPs in a wide temperature range (from room temperature to extremely high temperature). This circumvents the obstacles to the application of UCNPs in high-temperature sensing and extreme environmental lighting conditions.

Energy level regulation represents another fundamental approach to enhancing energy transfer efficiency. This strategy exhibits unique advantages and distinctly different implementation pathways in organic nanoparticle systems. A collaborative team from Japan and Soochow University[134] innovatively achieved precise energy level matching between charge transfer (CT) states and locally excited singlet (LE) states, successfully constructing an efficient upconversion pathway from CT to LE states.By precisely designing the molecular structure to reduce the energy difference between the CT and LE states, the team successfully promoted efficient energy transfer between the two states so that the luminescence efficiency and afterglow performance of the blue light-emitting long-afterglow material achieved a qualitative leap. The importance of this

breakthrough is that the resulting material met the stringent requirements of the international standard ISO 17398 class A (the highest class) for long-afterglow materials for emergency lighting for the first time, thus paving the way for the practical application of long afterglows in emergency indications, biological imaging, and other fields.

4. Biomedical applications of UCNPs

Owing to their unique photophysical properties, such as near-infrared excitation, anti-Stokes shift, tunable emission, excellent photostability, and low background interference, UCNPs have successfully overcome the key bottleneck of traditional optical probes in biomedical applications.[135] These materials not only serve as innovative tools for the high-resolution imaging of deep tissues but also show great potential in the fields of targeted therapy, multimodal diagnosis and treatment integration, and biosensing.[36,37,136]

4.1. Biological imaging

The pursuit of deeper and higher-fidelity *in vivo* optical imaging has driven the development of complementary nanoprobe strategies based on distinct photophysical principles. For maximizing universal imaging depth, downshifting nanoprobes with excitation in the NIR-I window and emission in the NIR-II window currently represent the mainstream approach, benefiting from reduced light scattering and absorption across both the incoming (excitation) and outgoing (emission) optical pathways.

In this context, upconversion nanoparticles (UCNPs) offer a fundamentally different paradigm. Their core value lies not in competing on universal depth, but in leveraging a unique combination of properties: the deep-tissue penetration of NIR excitation light coupled with the anti-Stokes emission process, which virtually eliminates tissue autofluorescence. This confers unparalleled capabilities for high-contrast imaging and sensing in scenarios where signal purity, photostability under prolonged illumination, and multiplexing capacity are paramount. This promising potential is fundamentally rooted in several intrinsic and unique advantages of UCNPs over conventional fluorophores.

First, ultra-low background and high signal-to-noise ratio (SNR). The extremely low autofluorescence background generated by biological tissues under NIR excitation, combined with the millisecond-long luminescence lifetime of UCNPs, enables effective filtering of short-lived background fluorescence using time-gated detection technology, thereby achieving ultra-high SNR imaging.[137,138] This feature greatly improves detection sensitivity and specificity and is especially suitable for capturing weak biological signals. For example, the SNR of ZnB-UCNPs can reach 8.75 in complex biological backgrounds, 38% higher than that of traditional materials, providing a new paradigm for the trace detection of biomarkers.[139]

Second, exceptional photostability. Comprising an inorganic matrix, UCNPs exhibit excellent resistance to photobleaching under prolonged light exposure.[140] This feature enables long-term dynamic observation of cells or biological processes, providing a powerful tool for studying dynamic life processes.[141,142]

Third, high functionalizability. The modifiable surface of UCNPs provides broad scope for functional expansion. Through surface functionalization, specific binding of UCNPs to target molecules (*e.g.*, antibodies, peptides) can be achieved, enabling precise targeted imaging of specific biomolecules or cells and further improving imaging specificity and accuracy.[36,143,144]

Together, these unique advantages have propelled the advancement of upconversion imaging, demonstrating significant value across many biomedical fields. *In vivo* imaging, particularly when combined with multimodal imaging and resolution enhancement techniques, continues to expand its application boundaries. For instance, core–shell upconversion nanorods ($NaYF_4$: Yb, Er@$NaYbF_4$@$NaYF_4$: Yb, Tm) capable of simultaneously emitting green (540 nm), red (655 nm), and blue (470 nm) light enable multicolor labeling and dynamic tracking of organelles.[145,146] At the whole-animal level, UCNP-based imaging technology has been successfully applied in key areas such as systemic vasculature visualization, accurate tumor boundary delineation, *in vivo* stem cell migration tracking, and lymphatic system imaging.[36,147] At the cellular and tissue levels, the high SNR provides a powerful tool for high-contrast organelle labeling, multiplexed target detection, and histopathological analysis even in samples with strong autofluorescence.[148–150]

Collectively, these advancements underscore that UCNP-based imaging technology, by virtue of its unparalleled SNR, multicolor encoding capability, and stability, is playing a significant and distinct role in specific cutting-edge domains of biomedical imaging. This opens new horizons for life science research and clinical applications, including the early diagnosis and treatment efficacy evaluation of various diseases.

4.2. Biodetection and biosensors

Because of their unique optical properties, UCNPs have become a research hotspot in the field of biosensors, exhibiting exceptional application potential. Their anti-Stokes luminescence fundamentally overcomes the key limitations of traditional fluorescent probes, such as organic dyes and quantum dots. NIR excitation can significantly reduce the background interference of autofluorescence in biological samples (such as cells, tissues, and blood), thereby improving the SNR and sensitivity by 1–3 orders of magnitude.[151] UCNPs also provide a reliable guarantee for long-term dynamic monitorin,[152] owing to their excellent photostability and absence of significant photobleaching. In addition, multi-color emission from ultraviolet to NIR light can be realized by precisely regulating the type and proportion of rare earth-doped ions, laying the foundation for the parallel detection of multiple targets.[153,154]

Currently, UCNPs have been widely integrated into various biosensor platforms to achieve highly sensitive and specific detection of biomarkers such as nucleic acids, proteins, small-molecule metabolites, metal ions, and pathogens, playing a key role in *in vitro* diagnosis, *in vivo* imaging tracing, point-of-

care testing (POCT) equipment development, and other fields.[55,153] This has promoted the development of early diagnostic devices, drug screening platforms, and precision medicine.

4.2.1. Detection of small molecular metabolites and trace pollutants. The ability of UCNPs to overcome background interference makes them useful for detecting small molecules at low concentrations. For example, to detect thiol compounds such as glutathione (GSH), Chu Long *et al.*[155] designed a composite of rare earth-doped UCNPs and MnO_2 nanosheets. MnO_2 can quench the fluorescence of UCNPs *via* energy transfer, while GSH can reduce MnO_2 to Mn^{2+} as a reducing agent. This resulted in a significant recovery of fluorescence and eventually achieved a detection limit of 31.2 nM, providing a highly sensitive tool for monitoring intracellular doxorubicin (DOX) levels. Jiang *et al.*[156] developed a dual-mode sensing platform based on UCNPs. Through the synergistic response of fluorescence signal changes and solution color differences, the detection limit of serum bilirubin was reduced to 21.4 nM; considering the detection sensitivity and visual reading requirements, this provides a new approach for the rapid screening of neonatal jaundice and other diseases. In addition to the above substances, UCNPs have also shown potential for detecting neurotransmitters such as dopamine and 5-hydroxytryptamine. By designing specific recognition groups (such as boric acid groups) to modify UCNPs, molecular interactions can be used to regulate the fluorescence intensity. *In situ* detection of neurotransmitters in the brain microenvironment can then be realized, providing a new method for studying the mechanisms of mental disorders and neurodegenerative diseases (Fig. 4).

4.2.2. Protein biomarker detection. In view of the stringent requirements for specificity and multiplicity in protein detection, the multi-color emission characteristics of UCNPs have become a core advantage of high-throughput immunoassays. Macala, J. *et al.*[157] developed a dot-blot immunoassay based on upconversion nanoparticles for the quantitative detection of human serum albumin (HSA); this assay had a detection limit of 0.19 ng mL^{-1} and a signal-to-background ratio of 722. Compared to traditional quantum-dot technology, it offers obvious advantages. This study demonstrated the value of upconversion nanomaterials for improving detection sensitivity. In a more innovative technique, Zhang *et al.*[158] used DNA-programmed UCNP-gold nanoparticle (AuNP) nanosatellite assemblies for the ultrasensitive detect tion of exosome proteins. By attaching three different aptamers to the gold nanoparticle core and an upconversion nanosatellite doped with different rare earth elements, the simultaneous detection of three exosome proteins was achieved, with a detection limit of 4.7×10^3 particles per mL (Fig. 4). The combination of UCNPs and nanozymes further expands the functional boundaries of protein detection. For example, the co-assembly of peroxide-active Fe_3O_4 nanoparticles with UCNPs can achieve ultrasensitive detection of tumor markers through the triple signal amplification of fluorescence, colorimetry, and catalysis, meeting the dual needs of accurate quantification in the laboratory and rapid screening at the point of care.[159,160]

4.2.3. Genetic diagnosis and pathogen screening. In the field of genetic diagnosis and pathogen screening, the high sensitivity and specificity elicited by UCNPs make them an ideal platform for the construction of nucleic acid sensors. By designing fluorescence resonance energy transfer (FRET)-based UCNP-DNA probes or combining them with nucleic acid amplification techniques, the ultrasensitive and rapid identification of specific gene sequences, mutations, or pathogenic nucleic acids has been achieved. For example, for SARS-CoV-2 viral RNA detection, FRET systems of UCNPs ($NaGdF_4$:Yb/Tm@$NaYF_4$:Yb/Er) and AuNPs were constructed to enhance energy transfer efficiency *via* local surface plasmon resonance. The detection limit was as low as 750 aM, shortening the detection time compared to that of traditional RT-PCR.[161]

In bacterial detection, the ADA-coated UCNPs@NB sensing platform combined with PCR technology can detect *Escherichia coli* cells *via* fluorescence quenching, with a detection limit of 33 colony-forming units (CFU) per mL, providing a new scheme for the rapid screening of foodborne pathogens.[162]

UCNPs also have potential applications in epigenetic testing, such as DNA methylation.[163,164] By designing methylation-specific primers and UCNP-labeled probes, fluorescence changes can be monitored in real time during the isothermal amplification process, the methylation level of tumor suppressor genes can be quantitatively analyzed, and a molecular marker detection tool can be used for early cancer risk assessment.

4.2.4. Dynamic monitoring of key ions *in vivo*. The deep-tissue penetration ability of UCNPs makes them ideal probes for the dynamic monitoring of ions *in vivo*. For example, HSA-modified LaF_3:Er, Yb UCNPs can emit green light (520/540 nm) and red light (655 nm) under 976-nm light excitation, and dynamic imaging of intracellular pH can be achieved through the change of the green/red fluorescence intensity ratio. At a treatment concentration of 0.4 mg mL^{-1}, the cell survival rate was more than 80%, indicating biocompatibility and deep penetration.[165] In calcium (Ca^{2+}) monitoring, UCNPs are combined with genetically encoded calcium indicators, such as GCaMP, to construct two-photon activation probes. These probes can capture neuronal calcium sparks with a temporal resolution of <100 ms, providing a tool with high spatial and temporal resolution for the real-time tracking of neural activity.[166] Nowadays, UCNPs can detect metal ions such as Zn^{2+} and Cu^{2+} *in vivo*. For example, through the modification of Zn^{2+}-specific chelators, such as diethyltriamine pentaacetic acid, UCNPs can be used to image Zn^{2+} *in situ* in zebrafish embryos under NIR light excitation, providing a visualization tool for studying the mechanism of metal ions during organismal development.[167,168]

4.2.5. Expanding to multi-functional platforms. The advantages of UCNPs are driving upgrades from single detection tools to multi-functional platforms. In the field of POCT, cucurbit uril was used to modify UCNPs with Huang *et al.*[169] to enhance its water solubility and antibody anchoring efficiency and reduce the detection limit of danofloxacin to 0.04 ng mL^{-1}. This limit is 20 times more sensitive than the traditional

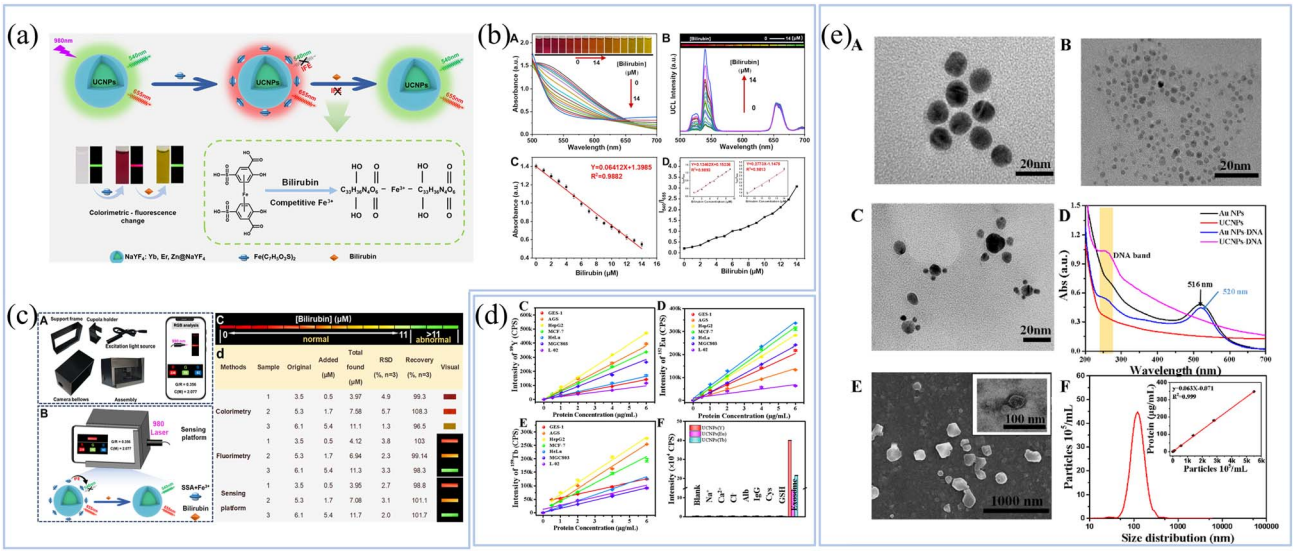

Fig. 4 (a) Schematic diagram of sensing mechanism of upconversion nanofluorescent sensor used for bilirubin detection. (b) (1) UV-vis absorption spectra of the probe solution as the bilirubin concentration increases. The illustration shows the color evolution of the probe solution after the addition of bilirubin. (2) Evolution of the UCL spectrogram of the nanoprobe (λ_{ex} = 980 nm) with increasing bilirubin concentration, illustrated by the UCL color change image after the addition of bilirubin. (c) (1) Physical pictures of the 3D-printed sensing platform. (2) Schematic diagram of a smartphone sensor platform used to detect bilirubin. (3) Fluorescence images corresponding to different concentrations of bilirubin in a serum environment and (4) recovery data of bilirubin detected in human serum based on luminescence, colorimetry, and smartphone sensor platform. (d) Dependence of ICP-MS counts for Y (C), Eu (D), and Tb (E) upon the concentration of target exosomes. (F) ICP-MS counts for the detection of 5 μg mL^{-1} exosomes with respect to those achieved without exosome but in the presence of Na^+ (150 mM), Ca^{2+} (150 mM), Cl^- (100 mM), Alb (50 mg mL^{-1}), IgG (20 mg mL^{-1}), Cys (10 mM), and GSH (50 mM). (e) (1–3) TEM images of AuNPs, UCNPs, and nanosatellite assemblies. (4) UV-vis of AuNPs, UCNPs, AuNP-DNA, and UCNP-DNA. (5) SEM and TEM images of exosomes. (6) NTA size distribution of exosomes and the relationship between protein concentration and particle number.[156,158] Figure description, reproduced from ref. 156 and 158 with permission from ACS Publications L. Zhang, X. Kang, F. Yang, W. Jia, L. Yang and C. Jiang, *Analytical Chemistry*, 2025, **97**, 3515–3524 & ACS Publications X.-W. Zhang, M.-X. Liu, M.-Q. He, S. Chen, Y.-L. Yu and J.-H. Wang, *Analytical Chemistry*, 2021, **93**, 6437–6445, Copyright 2025.

colloidal gold technology and is suitable for home self-testing or on-site screening.[169]

In the management of chronic diseases, Hu *et al.* 170 embedded UCNPs and *p*-dimethylamino cinnamaldehyde (*p*-DMAC) into a hydrogel and detected urea based on the internal filtration effect. The red product generated by the reaction of urea and *p*-DMAC can quench the green light emitted by UCNPs. Combined with RGB analysis using a smartphone, urea can be monitored in sweat/saliva in real time, providing support for the home management of chronic kidney disease (Fig. 5). In addition, UCNPs have a significant potential for the development of theranostics, integrating diagnosis and treatment.[171,172] The surface of UCNPs loaded with chemotherapeutic drugs (such as DOX) can simultaneously realize tumor-site imaging and light-controlled drug release under NIR light excitation. Through the synergy of imaging-guided precision drug delivery, the treatment efficiency can be improved and the toxic side effects can be reduced, providing a new strategy for precision cancer treatment.

In summary, UCNPs have achieved a leap from basic research to clinical applications in the field of biosensors, owing to their unique optical properties. In the future, with the optimization of material modification technology and the deepening of multidisciplinary integration, UCNPs are expected to make greater breakthroughs in the fields of single-cell analysis, *in vivo* dynamic monitoring, and diagnosis and treatment integration, providing more powerful tools for life science research and disease diagnosis and treatment.

4.3. Photodynamic therapy

Photodynamic therapy (PDT), which relies on photosensitizers, specific-wavelength light, and oxygen to produce reactive oxygen species (ROS) that kill tumor cells, has become an important approach in the field of cancer treatment.[173,174] However, traditional PDT faces three core challenges: the limited penetration depth of visible light (usually <1 cm),[175,176] which makes it difficult to target deep tumors; ubiquitous hypoxia in the tumor microenvironment,[177] which impairs the efficiency of ROS generation; and the immunosuppressive tumor microenvironment,[176,178] which leads to recurrence after treatment. UCNPs provide a new solution to break through these bottlenecks and promote the development of PDT in the direction of high efficiency, precision, and multi-modality with their anti-Stokes luminescence characteristics of NIR light excitation and visible light emission.

4.3.1. Innovation in photosensitizer activation mechanisms. The core advantage of UCNPs is that they can efficiently convert NIR light (such as 980 nm) with strong tissue penetration (penetration depth of up to several centimeters) into visible or ultraviolet light to remotely activate photosensitizers to produce ROS.[179] This photoconversion mechanism fundamentally solves the problem of the insufficient penetration of visible

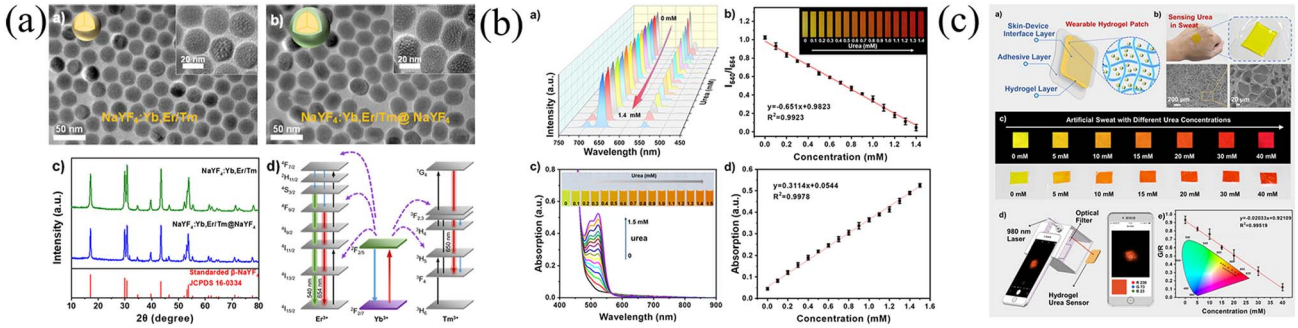

Fig. 5 (a) TEM images of (1) $NaYF_4$: Yb, Er/Tm core UCNPs and (2) $NaYF_4$: Yb, Er/Tm@$NaYF_4$ core–shell UCNPs. (3) X-ray diffraction patterns of the core particles and the core–shell particles, respectively. (d) Energy transfer mechanisms in UCNPs. (b) (1) Fluorescence spectra of the probe after the addition of urea (0–1.4 mM). (2) Linear fitting curve between I_{540}/I_{654} and urea concentration. (3) Absorption spectra of the probe after the addition of urea (0–1.5 mM). (d) Linear fitting curve between the urea concentration and the absorbance at 524 nm. (c) (1) Designed wearable hydrogel sensing patch. (2) Sensing urea in sweat and the SEM images of the hydrogel. (3) Response of the hydrogel sensing patch to urea under 980 nm excitation and daylight. (4) Designed portable sensing platform for urea determination. (5) Linear relationship between the ratio of G/R and concentrations of urea in the range of 0–40 mM.[170] Figure description, reproduced from ref. 170 with permission from ACS Publications B. Hu, X. Kang, S. Xu, J. Zhu, L. Yang and C. Jiang, *Analytical Chemistry*, 2023, https://doi.org/10.1021/acs.analchem.2c03806, Copyright 2025.

light in conventional PDT. Numerous *in vitro* and *in vivo* studies have demonstrated that UCNP- PDT remains highly effective in activating photosensitizers, generating reactive oxygen species (ROS), and inhibiting tumor growth, even when targeting tissues at depths of 1 centimeter or greater. This approach exhibits significantly enhanced therapeutic efficacy compared to conventional visible light-activated PDT.[180] Furthermore, the UCNP-PEG-FA/PC70 composite nanoparticles designed by Guan *et al.* [181] demonstrated the ingenious idea of co-design: folate (FA) ligand modification enhances tumor targeting and cell internalization efficiency, while UCNPs can convert NIR light to UV-visible light to activate the porphyrin-based photosensitizer PC70. This system can stably produce singlet oxygen and partially alleviate the inhibitory effects of tumor hypoxia on PDT, even in hypoxic environments. In addition to direct energy transfer, the spatially restricted design of UCNPs and photosensitizers can further improve the activation efficiency. For example, photosensitizers can be anchored in the mesoporous silica layer on the surface of UCNPs through covalent bonds. With this, the distance between the two particles can be controlled within the optimal energy transfer range of 1–10 nm, and the ROS yield becomes 2–3 times higher than that of the physical hybrid system. This provides a new idea for material design for efficient PDT. Beyond photosensitizer activation, UCNPs have also unlocked unique therapeutic opportunities in other modalities. The unique photoconversion capability of UCNPs establishes them as a versatile platform for multimodal therapy. This expansion beyond PDT underscores their versatility, as discussed in the following section on multimodal collaboration.[182]

4.3.2. Targeted delivery and precise activation. Tumor-targeted delivery of UCNPs through functional modification is the core method for improving the specificity of PDT and reducing normal tissue damage.[183,184] This process not only relies on the targeted identification of surface ligands but also achieves "double precision" through material structure optimization, which is not only targeted to be enriched in tumors but also activated only in the tumor microenvironment. At the material design level, the regulation of dopant ions and the core–shell structure is the key to improving overall performance. For example, UCNPs with a precision size adjustment (60.5 nm) and a three-layer core–shell structure ($NaYbF_4$:Er^{3+}@$NaGdF_4$:Yb^{3+}, Er^{3+}@$NaGdF_4$) showed a 30-fold increase in fluorescence intensity compared to the conventional structure; the outer Gd^{3+} layer enhanced magnetic resonance imaging contrast.[185] While exploring alternative activation strategies fordeep-seated tumors, researchers have also investigated stimuli beyond NIR light. For instance, Shchehlov and colleagues[186] developed a citric acid-modified Tb-doped hydroxyapatite (HA: Tb/Citr) particle loaded with a photosensitive RuBiNic complex, which can release nicotine under X-ray excitation (release rate of 4.17%), further breaking the penetration limit of NIR light. This work, although based on a different excitation mechanism (X-ray), underscores the broader pursuit of deep-tissue activation that motivates the development of NIR-driven UCNP platforms. This represents a new approach for the treatment of deep tumors (Fig. 6).

Moreover, the specific recognition of ligand modifications is particularly important in the targeting mechanism. Liu *et al.*[187] used FA-functionalized UCNP-RB nanocomplexes to precisely target folate receptor (FR)-positive JAR cancer cells. Upon irradiation with a 980 nm laser, the viability of JAR cells was significantly decreased, while FR-negative NIH3T3 cells were hardly affected, demonstrating a high targeting efficiency. The environment-responsive activation strategy can further improve accuracy. For example, a "smart switch" design that combines UCNPs with pH-sensitive polymers to release the photosensitizer only at the acidic conditions of the tumor microenvironment but remain stable in the neutral environment of normal tissue minimizes the risk of off-target activation[188] (Fig. 6).

It is difficult to eliminate tumors using PDT alone; hence, the multi-functional carrier characteristics of UCNPs make them an ideal platform for multi-therapy collaboration. By integrating chemotherapy, photothermal therapy, radiotherapy, and other

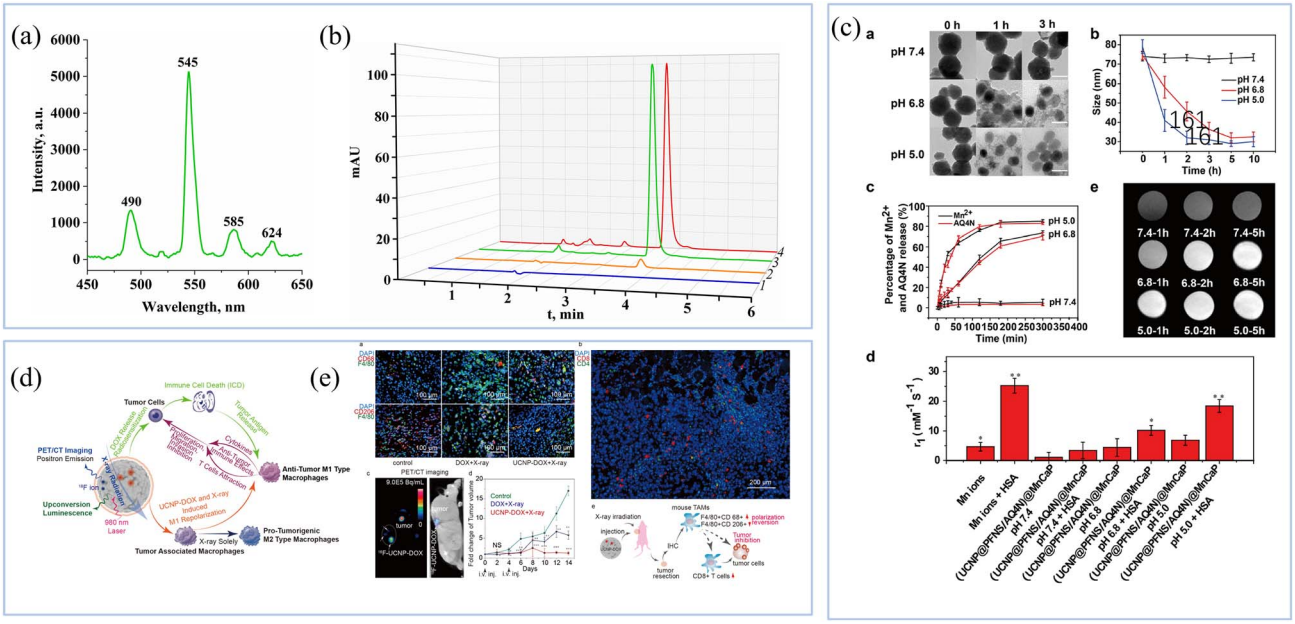

Fig. 6 (a) X-ray-induced luminescence spectrum of HA:Tb/Citr ScNPs; (b) shows typical chromatograms of solutions used for the quantitative determination of nicotine released under X-ray irradiation of HA:Tb/Citr ScNPs with surface-immobilized RuBiNic. (c) (1) TEM images showing the decomposition of the MnCaP shell of (UCNP@PFNS/AQ4N)@MnCaP at pH 7.4, 6.8 and 5.0 after 0, 1 and 3 h. (2) DLS of NPs at pH 5.0, 6.8 and pH 7.4 after 10 h. (3) The ratios of released from the initial loading amount of AQ4N and Mn^{2+} at pH 7.4, 6.8 and 5.0. (4) r1 relaxivity of (UCNP@PFNS/AQ4N)@MnCaP in physiological environments at different pH and with/without proteins (HSA). The interaction of Mn^{2+} ions released from (UCNP@PFNS/AQ4N)@MnCaP with HSA increased the relaxivity (r1). (5) MRI of (UCNP@PFNS/AQ4N)@MnCaP released at different pH in serum media (DMEM containing 10% fetal bovine serum (FBS)) measured by 7T MRI. (d) Mesoporous Bi-containing radiosensitizer loading with DOX to repolarize tumor-associated macrophages and elicit immunogenic tumor cell death to inhibit tumor progression. (e) *In vivo* antitumor immune effects of synergistic treatment of UCNP-DOX and X-ray. (1) Immunofluorescence imaging results of CD68, F4/80, and CD206 expression and (2) CD4 and CD8 expression in xenografted tumor of mice after intratumor injection of UCNP-DOX and X-ray radiation. (3) PET/CT images of the intratumorally injected fluorine-18-labeled UCNP-DOX. (d) Tumor volume growth curves after X-ray treatment alone (green), collaborative treatment of DOX and X-ray (blue), and collaborative treatment of UCNP-DOX and X-ray (red). (4) Schematic illustration of *in vivo* antitumor immune effects of synergistic treatment of UCNP-DOX and X-ray radiation.[186,188,191] Figure description, reproduced from ref. 186, 188 and 191 with permission from Hybrid Advances O. D. Shchehlov, A. P. Kusyak, A. L. Petranovska, D. I. Kravchuk, R. M. Kravchuk, Y. M. Shuba and P. P. Gorbyk, *Hybrid Advances*, 2025, 100530.& Wiley Y. Cai, X. Kang, L. Zhou, S. Wu, C. Wang, S. Wu, C. Huang, Q. Wang, Y. Chang and R. J. Babu, *Advanced Functional Materials*, 2025, 2425286 & Chemistry Europe T. Zhang, H. Lin, L. Cui, N. An, R. Tong, Y. Chen, C. Yang, X. Li, J. Liu and F. Qu, *European Journal of Inorganic Chemistry*, 2016, 1206–1213, Copyright 2025.

means, the therapeutic effect of "1 + 1 > 2" can be achieved.[189,190] The core–shell structure UCNP@mSiO_2 designed by Zhang *et al.*[191] is representative of this. They discovered that a mesoporous silica shell can simultaneously load the chemotherapeutic drug DOX and the photosensitizer chlorin (Ce6). Under NIR light irradiation, UCNPs can not only activate Ce6 to produce ROS through photoconversion but also promote the release of DOX through the photothermal effect to realize the synergy between PDT and chemotherapy (Fig. 6). More importantly, the X-ray attenuation property of rare earth ions can enhance the radiosensitivity of the system, which enables the system to have a PDT-chemotherapy-radiotherapy triple-killing ability and significantly improve the clearance efficiency of drug-resistant tumors. Interestingly, the introduction of immunomodulation has added a new dimension to multimodal treatments. For example, when UCNPs are loaded with tumor vaccines (such as tumor-associated antigens), PDT kills tumor cells and releases tumor-associated antigens, while the vaccines can synergistically activate dendritic cells, reverse the immunosuppressive tumor microenvironment, induce systemic anti-tumor immune responses, and reduce the risk of recurrence and metastasis.[192] This "PDT-immune" synergistic strategy is becoming an important development direction for the next generation of UCNP-based therapeutic systems.[193]

In summary, UCNPs have gradually overcome the inherent limitations of traditional PDT by improving the activation mode of photosensitizers, optimizing targeted delivery mechanisms, and constructing a multimodal synergistic system. In the future, with the refined design of material function and the maturity of clinical translation technology, UCNPs are expected to become core materials for the treatment of deep and drug-resistant tumors, promoting PDT from laboratory research to a new stage of clinical applications.

5. Summary and prospect

In the field of optical probes, UCNPs have successfully overcome the core bottlenecks of traditional optical probes, such as shallow tissue penetration and strong background interference, owing to their unique anti-Stokes property of NIR excitation and

visible/ultraviolet emission. In recent years, through material design innovations (such as core–shell structure optimization, lattice engineering regulation, surface modification) and energy transfer mechanism regulation (such as cascade sensitization strategy and collaborative doping technology), the luminous efficiency of UCNPs has been significantly improved. This is manifested by the generation of an optimized core–shell structure (*e.g.*, $LiYF_4$@$LiErF_4$@$LiYF_4$ @$LIYF_4$ multilayer structure) that increased the luminescence intensity 760-fold and achieved a quantum yield of 2.29% and the breaking of crystal symmetry by doping Ca^{2+}/Gd^{3+}, resulting in the increasing in red light emission intensity by 8-fold. Moreover, surface modification techniques, such as organic ligand coating, have improved the high-temperature stability of materials by six orders of magnitude.

Based on the aforementioned performance breakthroughs, UCNPs have demonstrated multidimensional application value in the biomedical field. Specifically, in the field of imaging, UCNPs have achieved a 2-fold increase in tissue penetration depth and an imaging resolution of 50 μm through NIR-II band (1532 nm) excitation and 3D printing technology. In biosensing, the FRET-based nanosatellite module can realize the simultaneous detection of multiple targets, with a detection sensitivity of 4.7×10^3 particles per mL and a detection limit of 31.2 nM for small molecular metabolites. In the field of PDT, UCNPs can remotely activate photosensitizers (such as the RuBiNic complex) using NIR light and integrate folic acid/RGD-modified targeted delivery systems with a PDT-chemotherapy-radiotherapy multimodal synergistic strategy to significantly improve the clearance efficiency of deep tumors.

To overcome the efficiency bottleneck, it is necessary to develop new sensitizers (*e.g.*, using Cr^{3+} to extend the excitation band to 800–900 nm) to reduce the excitation power requirement. At the same time, the PA mechanism and quantum confinement effects (in combination with COF material design) can be explored to improve the quantum yield to >24%. Furthermore, non-radiative energy loss can be reduced by optimizing the energy transfer path, such as by building a three-wire upconversion cascade system.

For biosafety and functional integration, it is necessary to clarify the long-term *in vivo* metabolic mechanisms of UCNPs and develop degradable matrix materials (such as MOF/fluorine oxide composites). Designing environment-responsive delivery systems (such as pH/enzyme-triggered delivery systems) can also be done to achieve the precise activation of diagnostic and therapeutic functions. At the same time, it can promote its immunomodulatory function and induce anti-tumor immune response *via* PDT to reduce the risk of tumor recurrence.

For clinical transformation and large-scale production, green synthesis processes, such as microfluidic-assisted co-precipitation and microwave thermal decomposition, should be developed to reduce production costs and improve batch stability. There is also a need to promote the integration of multimodal testing equipment (such as smartphone portable testing systems and 3D-printed implantable devices) to accelerate the clinical applications of POCT and personalized medicine.

6. Conclusions

Although significant progress has been made in the material design and biomedical applications of UCNP, their future development still crucially depends on key breakthroughs in interdisciplinary collaboration and clinical translation. Future research should focus on the following priorities: first, exploring novel sensitization mechanisms (*e.g.*, using Cr^{3+}, Mn^{2+}, *etc.*) to broaden the excitation spectrum and reduce power thresholds; second, systematically evaluating the long-term biosafety and metabolic pathways of UCNPs, and developing biodegradable rare-earth matrix systems; third, advancing the construction of intelligent, responsive UCNP systems to achieve precise control over imaging and therapeutic functions triggered by environmental cues; fourth, integrating advanced technologies such as microfluidics and artificial intelligence to overcome reproducibility and cost barriers in large-scale production. Only through cross-disciplinary innovation and collaboration can UCNPs truly transition from the laboratory to clinical practice, emerging as core components of next-generation theranostic platforms.

Author contributions

All authors have accepted responsibility for the entire content of this manuscript and approved its submission.

Conflicts of interest

There are no conflicts to declare.

Data availability

This article is a review and does not contain any original experimental data. All data referenced and discussed in this manuscript are available from publicly accessible sources, including peer-reviewed publications and scientifc databases, which are properly cited within the text. No new datasets were generated or analyzed during the current study.

Acknowledgements

The authors would like to thank the financial support provided by Central guidance for local scientific and technological development projects (2025YD022) for the publication of this paper.

Notes and references

1 H.-L. Yang, L.-F. Bai, Z.-R. Geng, H. Chen, L.-T. Xu, Y.-C. Xie, D.-J. Wang, H.-W. Gu and X.-M. Wang, *Mater. Today Adv.*, 2023, **18**, 100376.
2 Z. Yang, T. Xu, H. Li, M. She, J. Chen, Z. Wang, S. Zhang and J. Li, *Chem. Rev.*, 2023, **123**, 11047–11136.
3 Y. Guo and J. Li, *Mater. Sci. Eng. C*, 2020, **109**, 110511.
4 P. Reineck, A. Francis, A. Orth, D. W. M. Lau, R. D. V. Nixon-Luke, I. D. Rastogi, W. A. W. Razali, N. M. Cordina,

L. M. Parker and V. K. A. Sreenivasan, *Adv. Opt. Mater.*, 2016, **4**, 1549–1557.
5 A. H. Ashoka, I. O. Aparin, A. Reisch and A. S. Klymchenko, *Chem. Soc. Rev.*, 2023, **52**, 4525–4548.
6 D. Xiao, H. Qi, Y. Teng, D. Pierre, P. T. Kutoka and D. Liu, *Nanoscale Res. Lett.*, 2021, **16**, 167.
7 S. Kundu, M. Ghosh and N. Sarkar, *Langmuir*, 2021, **37**, 9281–9301.
8 Z. Jiang, X. Han, C. Zhao, S. Wang and X. Tang, *Int. J. Mol. Sci.*, 2022, **23**, 1923.
9 M. Díaz-González, A. de la Escosura-Muñiz, M. T. Fernandez-Argüelles, F. J. García Alonso and J. M. Costa-Fernandez, *Top. Curr. Chem.*, 2020, **378**, 35.
10 V. Naresh and N. Lee, *Sensors*, 2021, **21**, 1109.
11 E. Sheikhzadeh, V. Beni and M. Zourob, *Talanta*, 2020, **230**, 122026.
12 A. Uslu, S. O. Tümay and S. Yeşilot, *J. Photochem. Photobiol., C*, 2022, **53**, 100553.
13 P. Promcharoen, P. Chumkaeo, S. Charoenchaidet, S. Charoenchaidet and E. Somsook, *RSC Adv.*, 2025, **15**, 14420–14427.
14 P. Lu and J. Ai, *Talanta Open*, 2023, **8**, 100248.
15 Z. Sun, F. Yan, J. Xu, H. Zhang and L. Chen, *Nano Res.*, 2021, **15**, 414–422.
16 D. Svechkarev and A. M. Mohs, *Curr. Med. Chem.*, 2019, **26**, 4042–4064.
17 V. N. Mehta, M. L. Desai, H. Basu, R. K. Singhal and S. K. Kailasa, *J. Mol. Liq.*, 2021, **333**, 115950.
18 J. McKittrick and L. Shea-Rohwer, *J. Am. Ceram. Soc.*, 2014, **97**, 1327–1352.
19 Y. Liu, Z. Gui and J. Liu, *Polymers*, 2022, **14**, 851.
20 J. Sobhanan, J. V. Rival, A. Anas, E. S. Shibu, Y. Takano and V. Biju, *Adv. Drug Delivery Rev.*, 2023, **197**, 114830.
21 B. Omran, K. Whitehead and K. Baek, *Colloids Surf., B*, 2021, **200**, 111578.
22 W. Wu, Y. Yang, Y. Yang, Y. Yang, K. Zhang, L. Guo, H. Ge, X. Chen, J. Liu and H. Feng, *Small*, 2019, **15**, 1805549.
23 C. Gao, P. Zheng, Q. Liu, S. Han, D. Li, S. Luo, H. Temple, C. Xing, J. Wang and Y. Wei, *Nanomaterials*, 2021, **11**, 2474.
24 X. Zhu, J. Zhang, J. Liu and Y. Zhang, *Adv. Sci.*, 2019, **6**, 1901358.
25 R. Page, K. Schaffers, P. Waide, J. Tassano, S. Payne, W. Krupke and W. Bischel, *J. Opt. Soc. Am. B*, 1997, **15**, 996–1008.
26 L. Lyu, H. Cheong, X. Ai, W. Zhang, J. Li, H. Yang, J. Lin and B. Xing, *NPG Asia Mater.*, 2018, **10**, 685–702.
27 R. Stephens and R. A. McFarlane, *Opt Lett.*, 1993, **18**, 34–36.
28 A. Diening and S. Kück, *J. Appl. Phys.*, 2000, **87**, 4063–4068.
29 F. Auzel, *Chem. Rev.*, 2004, **104**, 139–174.
30 R. T. Wegh, H. Donker, K. D. Oskam and A. Meijerink, *Science*, 1999, **283**, 663–666.
31 G. S. Yi and G. M. Chow, *Adv. Funct. Mater.*, 2006, **16**, 2324–2329.
32 F. Li, L. Tu, Y. Zhang, D. Huang, X. Liu, X. Zhang, J. Du, R. Fan, C. Yang, K. W. Krämer, J. Marques-Hueso and G. Chen, *Nat. Photonics*, 2024, **18**, 440–449.
33 X. Li, X. Zhang, R. Chen, H. Liu, L. Wang, S. Cheng and Y. Yu, *Ceram. Int.*, 2024, **50**, 32171–32179.
34 C. Kang, S. Tao, F. Yang and B. Yang, *Aggregate*, 2022, **3**, e169.
35 H. Wang, Q. Li, P. Alam, H. Bai, V. Bhalla, M. Bryce, M. Cao, C. Chen, S. Chen, X. Chen, Y. Chen, Z. Chen, D. Dang, D. Ding, S. Ding, Y. Duo, M. Gao, W. He, X. He, X. Hong, Y. Hong, J. J. Hu, R. Hu, X. Huang, T. James, X. Jiang, G. Konishi, R. Kwok, J. Lam, C. Li, H. Li, K. Li, N. Li, W. J. Li, Y. Li, X.-J. Liang, Y. Liang, B. Liu, G. Liu, X. Liu, X. Lou, X. Lou, L. Luo, P. McGonigal, Z. Mao, G. Niu, T. C. Owyong, A. Pucci, J. Qian, A. Qin, Z. Qiu, A. Rogach, B. Situ, K. Tanaka, Y. Tang, B. Wang, D. Wang, J. Wang, W. Wang, W.-X. Wang, W.-J. Wang, X. Wang, Y.-F. Wang, S. Wu, Y. Wu, Y. Xiong, R. Xu, C. Yan, S. Yan, H. Yang, L. Yang, M. Yang, Y. Yang, J. Yoon, S. Zang, J. Zhang, P. Zhang, T. Zhang, X. Zhang, X. Zhang, N. Zhao, Z. Zhao, J. Zheng, L. Zheng, Z. Zheng, M. Zhu, W. H. Zhu, H. Zou and B. Z. Tang, *ACS Nano*, 2023, **17**, 14347–14405.
36 H. Li, H. Liu, K.-L. Wong and A. H. All, *Biomater. Sci.*, 2024, **12**, 4650–4663.
37 G. Liang, H. Wang, H. Shi, H. Wang, M. Zhu, A. Jing, J. Li and G. Li, *J. Nanobiotechnol.*, 2020, **18**, 154.
38 B. Liu, Y. Chen, C. Li, F. He, Z. Hou, S. Huang, H. Zhu, X. Chen and J. Lin, *Adv. Funct. Mater.*, 2015, **25**, 4717–4729.
39 B. Chen and F. Wang, *Accounts Chem. Res.*, 2020, **53**, 358–367.
40 C. Ma, C. Shan, K. Park, A. T. Mok, P. J. Antonick and X. Yang, *Nanophotonics*, 2020, **9**, 1993–2000.
41 X. Li, Y. Wang, J. Shi, Z. Zhao, D. Wang, Z. Chen, L. Cheng, G.-H. Lu, Y. Liang, H. Dong, X. Shan, B. Liu, C. Chen, Y. Liu, F. Liu, L.-D. Sun, X. Zhong and F. Wang, *Nano Lett.*, 2024, **24**, 5831–5837.
42 Z. Xu, Z. Huang, T. Jin, T. Lian and M. Tang, *Accounts Chem. Res.*, 2020, **54**, 70–80.
43 J.-A. Pan, X. Qi and E. M. Chan, *Nanoscale Horiz.*, 2025, **10**, 596–604.
44 S. P. Tiwari, S. K. Maurya, R. S. Yadav, A. Kumar, V. Kumar, M.-F. Joubert and H. C. Swart, *J. Vac. Sci. Technol. B*, 2018, **36**, 060801.
45 V. B. Pawade, N. R. Pawar and S. J. Dhoble, *Infrared Phys. Technol.*, 2022, **123**, 104148.
46 I. Șerban and A. Enesca, *Front. Chem.*, 2020, **8**, 354.
47 H. Li, G. Hou, Q. Tian, S. Bi, Z. Liu, Y.-Y. Lin, J. Tang and X.-J. Su, *Mater. Res. Express*, 2019, **6**, 045601.
48 S. Mohanty, M. Lederer, S. Premcheska, H. Rijckaert, K. De Buysser, E. Bruneel, A. Skirtach, K. Van Hecke and A. M. Kaczmarek, *J. Mater. Chem. C*, 2024, **12**, 11785–11802.
49 Y. Kaneko, K. Morimoto and T. Koda, *J. Phys. Soc. Jpn.*, 1982, **51**, 2247–2254.
50 S. Al-Ghamdi, A. Darwish, T. A. Hamdalla, A. O. M. Alzahrani, S. Khasim, S. I. Qashou and K. Abd El-Rahman, *Opt. Mater.*, 2022, **129**, 112514.
51 L. D. Carlos, R. A. S. Ferreira, V. d. Z. Bermudez and S. J. L. Ribeiro, *Adv. Mater.*, 2009, **21**, 509–534.
52 M. Wang, R. Dong and X. Feng, *Chem. Soc. Rev.*, 2021, **50**, 2764–2793.

53 J. Feng, Z. Xu, P. Dong, W. Yu, F. Liu, Q. Jiang, F. Wang and X. Liu, *J. Mater. Chem. B*, 2019, 7(6), 994–1004.
54 C. Duan, L. Liang, L. Li, R. Zhang and Z. Xu, *J. Mater. Chem. B*, 2018, **6**(2), 192–209.
55 J. Wu, J. Wu, W. Wei, Y. Zhang and Q. Chen, *Small*, 2024, **20**, 2311729.
56 K. Trejgis, A. Bednarkiewicz and L. Marciniak, *Nanoscale*, 2020, **12**, 4667–4675.
57 J. Sirucek, B. Le Guennic, Y. Damour, P.-F. Loos and D. Jacquemin, *J. Chem. Theory Comput.*, 2025, **21**, 4688–4703.
58 S. Jalilpiran, J. Lefebvre, Y. Messaddeq and S. LaRochelle, *Opt Lett.*, 2024, **49 20**, 5715–5718.
59 A. Prasad, A. Rao, M. Gupta and G. Prakash, *Mater. Chem. Phys.*, 2018, **219**, 13–21.
60 B. Amouroux, C. Wurth, C. Roux, A. Eftekhari, M. Sliwa, A. Bouchet, J.-C. Micheau, U. Resch Genger and C. Coudret, *J. Phys. Chem. C*, 2024, **128**, 18836–18848.
61 K. Prorok, M. Pawlyta, W. Stręk and A. Bednarkiewicz, *Chem. Mater.*, 2016, **28**, 2295–2300.
62 C. Mi, J. Wu, Y. Yang, B. Han and J. Wei, *Sci. Rep.*, 2016, **6**, 22545.
63 J. Huang, L. Yan, Z. An, H. Wei, C. Wang, Q. Zhang and B. Zhou, *Adv. Mater.*, 2024, **36**, 2310524.
64 J. Huang, L. Yan, Z. An, H. Wei, C. Wang, Q. Zhang and B. Zhou, *Adv. Mater.*, 2024, **36**, 2310524.
65 C. Meroni, S. Normani, C. Maunier, S. Montant, P. Camy and A. Braud, *Opt. Mater.*, 2024, **147**, 114664.
66 J. Du, S. Yang, Y. Qiao, H. Lu and H. Dong, *Biosens. Bioelectron.*, 2021, **191**, 113478.
67 C. Pedroso, C. Lee, E. Xu, V. Mann, E. Chan, P. J. Schuck and B. E. Cohen, *ECS Meeting Abstracts, Volume MA2022-02, D06: Quantum Dot Science and Technology 2*, The Electrochemical Society, 2022, vol. MA2022-02, p. 910.
68 A. Skripka, M. Lee, X. Qi, J.-A. Pan, H. Yang, C. Lee, P. J. Schuck, B. E. Cohen, D. Jaque and E. M. Chan, *Nano Lett.*, 2023, **23**, 7100–7106.
69 P. Dang, D. Liu, G. Li, A. A. Kheraif and J. Lin, *Adv. Opt. Mater.*, 2020, **8**, 1901993.
70 N. Ramadevi, R. Praveena, V. Venkatramu, C. Basavapoornima, V. Lavín and B. Joshi, *J. Korean Phys. Soc.*, 2022, **81**, 991–1003.
71 G. Sun, Y. Xie, Y. Wang, G. A. Mandl, S. L. Maurizio, H. Zhang, X. Ottenwaelder, J. A. Capobianco and L. Sun, *Angew. Chem., Int. Ed.*, 2023, **62**, e202304591.
72 H. S. Naher, B. A. H. Al-Turaihi, S. H. Mohammed, S. M. Naser, M. A. Albark, H. A. Madlool, H. A. M. Al-Marzoog and A. T. Jalil, *J. Drug Delivery Sci. Technol.*, 2023, **80**, 104175.
73 W. Rangel, R. A. B. Santa and H. Riella, *J. Mater. Res. Technol.*, 2020, **9**, 994–1004.
74 Y. Shen, Y. Wu, H. Xue, S. Wang, D. Yin, L. Wang and Y. Cheng, *ACS Appl. Mater. Interfaces*, 2021, **13**, 717–726.
75 T. Girardet, A. Cherraj, P. Venturini, H. Martinez, J.-C. Dupin, F. Cleymand and S. Fleutot, *Molecules*, 2024, **29**, 4484.
76 A. Apostoluk, Y. Zhu, P. Gautier, A. Valette, J.-M. Bluet, T. Cornier, B. Masenelli and S. Daniele, *Materials*, 2023, **16**, 5400.
77 M. Pudovkin, S. Korableva, D. Koryakovtseva, E. Lukinova, A. Lovchev, O. Morozov and V. Semashko, *J. Nanopart. Res.*, 2019, **21**, 266.
78 J. Granados-Reyes, A. C. Rueda and Y. Cesteros, *Appl. Clay Sci.*, 2024, **261**, 107590.
79 W. Hua, M. Chen, B. Schwarz, M. Knapp, M. Bruns, J. Barthel, X. Yang, F. Sigel, R. Azmi and A. Senyshyn, *Adv. Energy Mater.*, 2019, **9**, 1803094.
80 L. Panariello, M. O. Besenhard, S. Damilos, A. Sergides, V. Sebastian, S. Irusta, J. Tang, N. T. K. Thanh and A. Gavriilidis, *Chem. Eng. Process. Process Intensif.*, 2022, **182**, 109198.
81 D. Bokov, A. Turki Jalil, S. Chupradit, W. Suksatan, M. Javed Ansari, I. H. Shewael, G. H. Valiev and E. Kianfar, *Adv. Mater. Sci. Eng.*, 2021, **2021**, 5102014.
82 D. Navas, S. Fuentes, A. Castro-Alvarez and E. Chavez-Angel, *Gels*, 2021, **7**, 275.
83 N. Balighieh, S. Kashani-Bozorg, M. Kheradmandfard and M. R. Barati, *J. Mater. Sci.*, 2023, **58**, 17066–17079.
84 L. Predoană, G. Petcu, S. Preda, J. Pandele-Cuşu, S. V. Petrescu, A. Băran, N. G. Apostol, R. M. Costescu, V.-A. Surdu and B. Ş. Vasile, *Gels*, 2023, **9**, 267.
85 S. Zeng, C. Qin, F. Mo, P. Li and Z. Mo, *Mater. Lett.*, 2025, **382**, 137834.
86 T. D. Cao, T. G. Le, S. Turrell, M. Ferrari, Q. V. Lam and T. V. Tran, *Molecules*, 2021, **26**, 1041.
87 G. B. Nair, S. Tamboli, R. Kroon and H. Swart, *Mater. Today Chem.*, 2023, **29**, 101463.
88 T. Glazunova, A. Boltalin and P. Fedorov, *Russ. J. Inorg. Chem.*, 2006, **51**, 983–987.
89 Y.-W. Zhang, X. Sun, R. Si, L.-P. You and C.-H. Yan, *J. Am. Chem. Soc.*, 2005, **127**, 3260–3261.
90 Z. Wan, D. Zhang, C. Gao, M. Lu, Z. Li, Z. Huang, Y. You and Z. Wang, *Polym. Degrad. Stab.*, 2024, **222**, 110697.
91 A. Kmita, C. Fischer, K. Hodor, M. Holtzer and A. Roczniak, *Arab. J. Chem.*, 2016, **11**, 380–387.
92 Y. J. Liang, Y. Zhang, Z. Guo, J. Xie, T. Bai, J. Zou and N. Gu, *Chem.–Eur. J.*, 2016, **22**, 11807–11815.
93 J. Máčala, S. Kuusinen, S. Lahtinen, H. H. Gorris, P. Skládal, Z. Farka and T. Soukka, *Anal. Chem.*, 2025, **97**, 1775–1782.
94 G. Pang, Y. Zhang, X. Wang, H. Pan, X. Zhang, Y. Li, S. Zhang, C.-H. Yan, L.-D. Sun, H. Wang and J. Chang, *Nano Today*, 2021, **40**, 101264.
95 S. Shikha, X. Zheng and Y. Zhang, *Nano-Micro Lett.*, 2018, **10**, 31.
96 J. Ren, C. Li, X. Ji, G. Meng, S. Shi and S. Zhang, *Opt. Mater.*, 2025, **160**, 116712.
97 D. Le, M. Kreivi, S. Aikio, N. Heinilehto, T. Sipola, J. Petäjä, T.-L. Guo, M. Roussey and J. Hiltunen, *Nanophotonics*, 2024, **13**, 3995–4006.
98 J. Matias, K. Komolibus, S. Konugolu-Venkata-Sekar and S. Andersson-Engels, *Nanoscale*, 2022, **14**, 2230–2237.
99 E. Hemmer, A. Benayas, F. Légaré and F. Vetrone, *Nanoscale Horiz.*, 2016, **1**, 168–184.

100 F. Huang, N. Bagheri, L. Wang, H. Ågren, J. Zhang, R. Pu, Q. Zhan, Y. Jing, W. Xu and J. Widengren, *J. Am. Chem. Soc.*, 2023, **145**, 17621–17631.
101 J. Chen, L. Liang, S. Tan, S. Xi, C.-H. Lin, T. Wu, Q. He and X. Liu, *Nano Lett.*, 2023, **23**, 7221–7227.
102 J. P. Jonasse, M. P. Perich, S. J. Turner and J. E. van der Hoeven, *Nanoscale*, 2025, **17**, 7100–7113.
103 S. Geng, H. Li, Z. Lv, Y. Zhai, B. Tian, Y. Luo, Y. Zhou and S. T. Han, *Adv. Mater.*, 2025, 2419678.
104 S. Zhang, X. Hu, P. Huang, X. Shang, D. Yang, Z. Shao, X. Wang, W. Zheng and X. Chen, *Nano Lett.*, 2025, **25**, 7426–7434.
105 Y. Niu, Z. Bao, Y. Gao, M. Guo, J. Liu, J. Shao, M. Lu, Z. Yuan and X. Xie, *J. Rare Earths*, 2024, **42**, 947–954.
106 Z.-J. Yong, S. Guo, P. Ju, J.-Y. Zhang, Z.-Y. Li, Y.-M. Chen, B.-B. Zhang, Y. Zhou, J. Shu, J.-L. Gu, L.-R. Zheng, O. Bakr and H. T. Sun, *J. Am. Chem. Soc.*, 2018, **140 31**, 9942–9951.
107 H. Wu, J. Pi, D. Zhou, Q. Wang, Z. Long and J. Qiu, *Ceram. Int.*, 2022, **48**, 3383–3389.
108 T. Wang, L. Xu, Z. Wu, Y. Li, Z. Yin, J. Han, Z. Yang, J. Qiu and Z. Song, *Nanoscale*, 2022, **14**, 12909–12917.
109 Y. Shang, S. Hao, W. Shao, T. Chen, Y. Zhu and C. Yang, *J. Mater. Chem. C*, 2020, **8**, 2847–2851.
110 S. Pei, X. Ge and L. Sun, *Front. Chem.*, 2020, **8**, 610481.
111 X. Guo, X. Yang and S. Xiao, *Opt. Mater.*, 2025, **158**, 116442.
112 B. Yu, X. Zhou, X. Tang, Y. Lin and C. Tang, *J. Sol-Gel Sci. Technol.*, 2020, **93**, 473–478.
113 W. Xie, X. An, L. Chen, J. Li, J. Leng, W. Lǔ, L. Zhang and Y. Luo, *Mater. Res. Bull.*, 2017, **95**, 509–514.
114 D. Zhu, J. Hu, K. Guo, Y. Wu, C. Ding, R. Fan, T. Liu, W. Jin and Y. Liu, *Opt. Mater.*, 2025, 117224.
115 W. Zhang, W. Zheng, P. Huang, D. Yang, Z. Shao, W. Zhang, H. Zhang, Z. Xie, J. Xu and X. Chen, *Nat. Commun.*, 2025, **16**, 6762.
116 L. Liang, J. Li, J. Ning, Y. Wang, B. Zu and X. Dou, *Cell Rep. Phys. Sci.*, 2025, **6**, 102721.
117 Y. Xin, J. Wang, X. Gao, Y. Yang, J. Zhang, J. Tang and Z. Zhang, *Adv. Mater.*, 2025, 2501658.
118 T. Cai, W. Shi, R. Wu, C. Chu, N. Jin, J. Wang, W. Zheng, X. Wang and O. Chen, *J. Am. Chem. Soc.*, 2024, **146**, 3200–3209.
119 L. Wang, T. Huang, R. Hou and B. Yang, *Appl. Phys. Lett.*, 2025, **126**, 063501.
120 C. Zhang, W. Su, J. Sun, Y. Man, Y. Wei, C. Duan, C. Han and H. Xu, *Adv. Mater.*, 2025, 2502747.
121 S. Li, K. Li, C. Yi, X. Gao and Z. Gan, *Nat. Commun.*, 2025, **16**, 6449.
122 T. Zhang, L. Liu, R. Wang, W. Zhang, X. Liu, C. Yuan and R. Hua, *RSC Adv.*, 2023, **13**, 9273–9280.
123 M. Matulionyte, A. Skripka, A. Ramos-Guerra, A. Benayas and F. Vetrone, *Chem. Rev.*, 2023, **123**, 515–554.
124 X. Zhou, W. Geng, J. Li, Y. Wang, J. Ding and Y. Wang, *Adv. Opt. Mater.*, 2020, **8**, 1902003.
125 Y. Sun, X. Zhong and A. M. Dennis, *J. Biomed. Opt.*, 2023, **28**, 094805.
126 M. Alkahtani, B. Alshehri, H. Alrashood, L. Alshehri, Y. A. Alzahrani, S. Alenzi, I. S. Almalki, G. S. Yafi, A. M. Alessa and F. S. Alghannam, *Molecules*, 2025, **30**, 2166.
127 L. Z. Pang, W. J. Lim, B. T. W. Ang, H. An, S.-C. Chien and C. B. Soh, *Renewable Sustainable Energy Rev.*, 2025, **5**, 1–7.
128 Y. Lei, M. Sakakura, L. Wang, Y. Yu, H. Wang, G. Shayeganrad and P. G. Kazansky, *Optica*, 2021, **8**, 1365–1371.
129 H. Wang, Y. Lei, L. Wang, M. Sakakura, Y. Yu, G. Shayeganrad and P. G. Kazansky, *Laser Photon. Rev.*, 2022, **16**, 2100563.
130 Y. Wu, Q. Liang, H. Zhu, X. Dai, B. B. Yu, Y. Hu, M. Chen, L. B. Huang, S. M. Zakeeruddin and Z. Shen, *Adv. Funct. Mater.*, 2023, **33**, 2302404.
131 C. Sun, C. Q. Jing, D. Y. Li, M. H. Dong, M. X. An, Z. H. Zhang, C. Y. Yue, H. Fei and X. W. Lei, *Adv. Sci.*, 2025, **12**, 2412459.
132 R. Gao, Y. Li, Y. Zhang, L. Fu and L. Li, *Nanomaterials*, 2024, **14**, 1969.
133 H. Suo, P. Zhao, X. Zhang, Y. Guo, D. Guo, J. Chang, J. Chen, P. Li, Z. Wang and H. Wei, *Nat. Commun.*, 2025, **16**, 3249.
134 Z. Lin, J. Ye, S. Shinohara, Y. Tanaka, R. Yoshioka, C.-Y. Chan, Y.-T. Lee, X. Tang, K. Mitrofanov and K. Wang, *Nat. Commun.*, 2025, **16**, 2686.
135 M. K. Mahata, R. De and K. T. Lee, *Biomedicines*, 2021, **9**, 756.
136 Y. Zhang, X. Zhu and Y. Zhang, *ACS Nano*, 2021, **15**, 3709–3735.
137 J. Han, S. Kim, D. Kang, S.-H. Lee, A. Y. Cho, H. Lee, J.-H. Kwon, Y. Shin, Y.-P. Kim and J. Lee, *ACS Sens.*, 2025, **10**, 1312–1320.
138 H. Li, M. Tan, X. Wang, F. Li, Y. Zhang, L. Zhao, C. Yang and G. Chen, *J. Am. Chem. Soc.*, 2020, **142**, 2023–2030.
139 X. Zhu, H. Li, Y. Liu, X. Dou and B. Zu, *ACS Appl. Nano Mater.*, 2025, **8**, 9903–9911.
140 Y. Li, C. Chen, F. Liu and J. Liu, *Microchim. Acta*, 2022, **189**, 109.
141 J. o. F. Shida, K. Ma, H. W. Toll, O. Salinas, X. Ma and C. S. Peng, *Nano Lett.*, 2024, **24**, 4194–4201.
142 O. Dukhno, S. Ghosh, V. Greiner, S. Bou, J. Godet, V. Muhr, M. Buchner, T. Hirsch, Y. Mely and F. Przybilla, *ACS Appl. Mater. Interfaces*, 2024, **16**, 11217–11227.
143 C. C. Pedroso, V. R. Mann, K. Zuberbühler, M.-F. Bohn, J. Yu, V. Altoe, C. S. Craik and B. E. Cohen, *ACS Nano*, 2021, **15**, 18374–18384.
144 N. Akhtar, P.-W. Wu, C. L. Chen, W.-Y. Chang, R.-S. Liu, C. T. Wu, A. Girigoswami and S. Chattopadhyay, *ACS Appl. Nano Mater.*, 2022, **5**, 7051–7062.
145 S. Liu, L. Yan, J. Huang, Q. Zhang and B. Zhou, *Chem. Soc. Rev.*, 2022, **51**, 1729–1765.
146 H. Jia, D. Li, D. Zhang, Y. Dong, S. Ma, M. Zhou, W. Di and W. Qin, *ACS Appl. Mater. Interfaces*, 2021, **13**, 4402–4409.
147 X. Xie, W. Liu, W. Zhu, G. Zhang, Y. Dai, J. Wu, H. Nie and L. Lei, *J. Biomed. Mater. Res.*, 2022, **110**, 1881–1891.
148 Z. Farka, M. J. Mickert, Z. Mikušová, A. Hlaváček, P. Bouchalová, W. Xu, P. Bouchal, P. Skládal and H. H. Gorris, *Nanoscale*, 2020, **12**, 8303–8313.

149 G. Liu, J. Wei, X. Li, M. Tian, Z. Wang, C. Shen, W. Sun, C. Li, X. Li and E. Lv, *Adv. Sci.*, 2022, **9**, 2202505.
150 J. Macala, S. Kuusinen, S. Lahtinen, H. H. Gorris, P. Skládal, Z. Farka and T. Soukka, *Anal. Chem.*, 2025, **97**, 1775–1782.
151 A. Ansari, V. Thakur and G. Chen, *Coord. Chem. Rev.*, 2021, **436**, 213821.
152 H. Rabie, Y. Zhang, N. Pasquale, M. J. Lagos, P. E. Batson and K. B. Lee, *Adv. Mater.*, 2019, **31**, 1806991.
153 H. Li, Y. Wu, M. Shoaib, W. Sheng, Q. Bei and A. Murugesan, *Chemosensors*, 2025, **13**, 60.
154 F. Pini, L. Frances-Soriano, V. Andrigo, M. M. Natile and N. Hildebrandt, *ACS Nano*, 2023, **17**, 4971–4984.
155 C. Long, K. Wu, M. Wang, L. Wang, Q. Zeng, T. Li and Q. Diao, *New J. Chem.*, 2025, **49**, 15038–15047.
156 L. Zhang, X. Kang, F. Yang, W. Jia, L. Yang and C. Jiang, *Anal. Chem.*, 2025, **97**, 3515–3524.
157 J. Macala, E. Makhneva, A. Hlavacek, M. Kopecky, H. H. Gorris, P. Skládal and Z. Farka, *Anal. Chem.*, 2024, **96**, 10237–10245.
158 X.-W. Zhang, M.-X. Liu, M.-Q. He, S. Chen, Y.-L. Yu and J.-H. Wang, *Anal. Chem.*, 2021, **93**, 6437–6445.
159 Y. Liang, Y. Liu, P. Lei, Z. Zhang and H. Zhang, *Nano Res.*, 2023, **16**, 9826–9834.
160 S. Fu, S. Wang, X. Zhang, A. Qi, Z. Liu, X. Yu, C. Chen and L. Li, *Colloids Surf., B*, 2017, **154**, 239–245.
161 X. Lao, Y. Liu, L. Li, M. Song, Y. Ma, M. Yang, G. Chen and J. Hao, *Aggregate*, 2024, **5**, e448.
162 Y. Song, M. Chen, L. Han, Z. Yan, L. Pan and K. Tu, *Anal. Chim. Acta*, 2023, **1239**, 340751.
163 Y. Zhou, W. Ma, R. Sun, B. Liu, X. Zhang and H. Yang, *Biosens. Bioelectron.*, 2022, **214**, 114549.
164 X. Yu, H. Zhao, R. Wang, Y. Chen, X. Ouyang, W. Li, Y. Sun and A. Peng, *Cell Death Discov.*, 2024, **10**, 28.
165 P. Deshmukh, B. Sharma, S. Chakraborty, H. Srivastava, K. Sahu, S. Satapathy and S. K. Majumder, *Luminescence*, 2025, **40**, e70269.
166 J. Wu, T. Saizaki, T. Yoshinobu and Y. Guo, *Talanta*, 2025, **285**, 127249.
167 Z. Yang, K. Loh, Y. Chu, R. Feng, N. S. R. Satyavolu, M. Xiong, S. N. Huynh, K. Hwang, L. Li, H. Xing, X. Zhang, Y. Chemla, M. Gruebele and Y. Lu, *J. Am. Chem. Soc.*, 2018, **140 50**, 17656–17665.
168 C. Hao, R. Gao, Y. Li, L. Xu, M. Sun, C. Xu and H. Kuang, *Angew. Chem.*, 2019, **131**, 7449–7452.
169 Z. Huang, Y. Liu, Y. Chen, Q. Xiong, Y. Wang, H. Duan and W. Lai, *Sens. Actuators, B*, 2020, **318**, 128233.
170 B. Hu, X. Kang, S. Xu, J. Zhu, L. Yang and C. Jiang, *Anal. Chem.*, 2023, **95**, 3587–3595.
171 G. Jin, R. He, Q. Liu, M. Lin, Y. Dong, K. Li, B. Z. Tang, B. Liu and F. Xu, *Theranostics*, 2019, **9**, 246.
172 G. Y. Erdem, B. Goncu, S. Atasoy, A. Y. Uysal, S. Dag and A. Dag, *J. Mater. Chem. B*, 2025, **13**, 2150–2166.
173 J. H. Correia, J. A. Rodrigues, S. Pimenta, T. Dong and Z. Yang, *Pharmaceutics*, 2021, **13**, 1332.
174 G. Gunaydin, M. E. Gedik and S. Ayan, *Front. Chem.*, 2021, **9**, 691697.
175 B. Sun, J. N. B. Rahmat and Y. Zhang, *Biomaterials*, 2022, **291**, 121875.
176 W. Zhao, L. Wang, M. Zhang, Z. Liu, C. Wu, X. Pan, Z. Huang, C. Lu and G. Quan, *MedComm*, 2024, **5**, e603.
177 W. Jiang, M. Liang, Q. Lei, G. Li and S. Wu, *Cancers*, 2023, **15**, 585.
178 R. V. Huis in 't Veld, J. Heuts, S. Ma, L. J. Cruz, F. A. Ossendorp and M. J. Jager, *Pharmaceutics*, 2023, **15**, 330.
179 Z. Wei, X. Liu, D. Niu, L. Qin and Y. Li, *ACS Appl. Bio Mater.*, 2020, **3**(7), 4655–4664.
180 K. Mironova, D. Khochenkov, A. Generalova, V. Rocheva, N. Sholina, A. Nechaev, V. Semchishen, S. Deyev, A. Zvyagin and E. Khaydukov, *Nanoscale*, 2017, **9**(39), 14921–14928.
181 M. Guan, H. Dong, J. Ge, D. Chen, L. Sun, S. Li, C. Wang, C. Yan, P. Wang and C. Shu, *NPG Asia Mater.*, 2015, **7**, e205.
182 E. Carrasco, B. del Rosal, F. Sanz-Rodríguez, Á. J. de la Fuente, P. H. Gonzalez, U. Rocha, K. U. Kumar, C. Jacinto, J. G. Solé and D. Jaque, *Adv. Funct. Mater.*, 2015, **25**, 615–626.
183 B. Ling, Y. Wang, H. Dong, H. Chen and L. Wang, *Nanoscale Adv.*, 2025, **7**, 3068–3076.
184 B. Ling, L. Yang, C. Wang, L. Dong, Y. Yang, L. Wang, J. Zhang and Y. Yuan, *ACS Mater. Lett.*, 2024, **6**, 5256–5265.
185 S. Ghosh, M. Deshpande, P. Xu, R. Shinde, W.-S. Chae, S.-H. Kwon, J.-Y. Jeon, K. S. Hong, C. Y. Park and Y. H. Kim, *Colloids Surf., B*, 2025, 114919.
186 O. D. Shchehlov, A. P. Kusyak, A. L. Petranovska, D. I. Kravchuk, R. M. Kravchuk, Y. M. Shuba and P. P. Gorbyk, *Hybrid Adv.*, 2025, 100530.
187 K. Liu, Functionalized upconversion nanoparticles for cancer imaging and therapy, Universiteit van Amsterdam, 2014.
188 Y. Ji, F. Lu, W. Hu, H. Zhao, Y. Tang, B. Li, X. Hu, X. Li, X. Lu and Q. Fan, *Biomaterials*, 2019, **219**, 119393.
189 Y. Cai, X. Kang, L. Zhou, S. Wu, C. Wang, S. Wu, C. Huang, Q. Wang, Y. Chang and R. J. Babu, *Adv. Funct. Mater.*, 2025, 2425286.
190 M. Żuk, W. Gawęda, A. Majkowska-Pilip, M. Osial, M. Wolski, A. Bilewicz and P. Krysiński, *Pharmaceutics*, 2021, **13**, 1843.
191 T. Zhang, H. Lin, L. Cui, N. An, R. Tong, Y. Chen, C. Yang, X. Li, J. Liu and F. Qu, *Eur. J. Inorg. Chem.*, 2016, **2016**, 1206–1213.
192 X. Qin, J. Liu, Y. Xu, B. Li, J. Cheng, X. Wu, J. Zhang, Z. Liu, R. Ning and Y. Li, *ACS Appl. Mater. Interfaces*, 2020, **12**, 31225–31234.
193 F. Jin, J. Qi, D. Liu, Y. You, G. Shu, Y. Du, J. Wang, X. Xu, X. Ying and J. Ji, *J. Controlled Release*, 2021, **337**, 90–104.